Evolution of immunity to SARS-CoV-2

Adam K. Wheatley[1,2]*, Jennifer A. Juno[1]*, Jing J. Wang[3]*, Kevin J. Selva[1], Arnold Reynaldi[4], Hyon-Xhi Tan[1], Wen Shi Lee[1], Kathleen M. Wragg[1], Hannah G. Kelly[1,2], Robyn Esterbauer[1,2], Samantha K. Davis[1], Helen E. Kent[1,5], Francesca L. Mordant[1], Timothy E. Schlub[4,6], David L. Gordon[7], David S. Khoury[4], Kanta Subbarao[1,8], Deborah Cromer[4], Tom P. Gordon[3,9], Amy W. Chung[1], Miles P. Davenport[4], Stephen J. Kent[1,2,5]✉.

*AKW, JAJ and JJW contributed equally

[1] Department of Microbiology and Immunology, University of Melbourne, at The Peter Doherty Institute for Infection and Immunity, Melbourne, Victoria, Australia

[2] Australian Research Council Centre for Excellence in Convergent Bio-Nano Science and Technology, University of Melbourne, Melbourne, Victoria, Australia

[3] Department of Immunology and Flinders Proteomics Facility, College of Medicine and Public Health, Flinders University, Adelaide, South Australia, Australia

[4] Kirby Institute, University of New South Wales, Kensington, New South Wales, Australia

[5] Melbourne Sexual Health Centre and Department of Infectious Diseases, Alfred Hospital and Central Clinical School, Monash University, Melbourne, Victoria, Australia

[6] Sydney School of Public Health, Faculty of Medicine and Health, University of Sydney, Sydney, New South Wales, Australia

[7] Department of Microbiology and Infectious Diseases, Flinders University and SA Pathology, Flinders Medical Centre, Adelaide, South Australia, Australia

[8] WHO Collaborating Centre for Reference and Research on Influenza, The Peter Doherty Institute for Infection and Immunity, Melbourne, Victoria, Australia

[9] Department of Immunology, SA Pathology, Flinders Medical Centre, Adelaide, South Australia, Australia

✉ Corresponding author. Address to Professor Stephen Kent, Department of Microbiology and Immunology, Doherty Institute, 792 Elizabeth St, Melbourne, Victoria, Australia 3000. Phone +61 3 8344 9939. Email: skent@unimelb.edu.au

40
41 The durability of infection-induced SARS-CoV-2 immunity has major implications
42 for public health mitigation and vaccine development. Animal studies[1,2] and the
43 scarcity of confirmed re-infection[3] suggests immune protection is likely, although the
44 durability of this protection is debated. Lasting immunity following acute viral
45 infection requires maintenance of both serum antibody and antigen-specific memory
46 B and T lymphocytes and is notoriously pathogen specific, ranging from life-long for
47 smallpox or measles[4], to highly transient for common cold coronaviruses (CCC)[5].
48 Neutralising antibody responses are a likely correlate of protective immunity and
49 exclusively recognise the viral spike (S) protein, predominantly targeting the receptor
50 binding domain (RBD) within the S1 sub-domain[6]. Multiple reports describe waning
51 of S-specific antibodies in the first 2-3 months following infection[7-12]. However,
52 extrapolation of early linear trends in decay might be overly pessimistic, with several
53 groups reporting that serum neutralisation is stable over time in a proportion of
54 convalescent subjects[8,12-17]. While SARS-CoV-2 specific B and T cell responses are
55 readily induced by infection[6,13,18-24], the longitudinal dynamics of these key memory
56 populations remains poorly resolved. Here we comprehensively profiled antibody, B
57 and T cell dynamics over time in a cohort recovered from mild-moderate COVID-19.
58 We find that binding and neutralising antibody responses, together with individual
59 serum clonotypes, decay over the first 4 months post-infection, as expected, with a
60 similar decline in S-specific CD4+ and circulating T follicular helper (cTFH)
61 frequencies. In contrast, S-specific IgG+ memory B cells (MBC) consistently
62 accumulate over time, eventually comprising a significant fraction of circulating
63 MBC. Modelling of the concomitant immune kinetics predicts maintenance of
64 serological neutralising activity above a titre of 1:40 in 50% of convalescent subjects
65 to 74 days, with probable additive protection from B and T cells. Overall, our study

66 suggests SARS-CoV-2 immunity after infection is likely to be transiently protective at
67 a population level. SARS-CoV-2 vaccines may require greater immunogenicity and
68 durability than natural infection to drive long-term protection.
69
70 We recruited a longitudinal cohort of 64 subjects who recovered from COVID-19
71 (Extended Data Fig 1). A total of 158 samples were collected between day 26 and 149
72 post-symptom onset, with samples nominally denoted as early (≤50days),
73 intermediate (50-100 days) and late (≥100 days) convalescence (Fig 1A). In early
74 convalescence, neutralisation activity was widespread with a median serological titre
75 of 52, which declined to 34 in late convalescence (Fig 1B). A mixed-effects
76 modelling approach found that a two-phase decay model best fit with the observed
77 decay of neutralisation titres across the cohort ($p< 0.00001$, likelihood ratio test), with
78 rapid decay evident over the first half of our time-series (half-life ($t_{1/2}$) prior to day 70
79 = 55 days), compared with slower decay in the second half ($t_{1/2}$ from day 70 = 519
80 days)(Fig 1B). The capacity of immune plasma to inhibit interaction of the SARS-
81 CoV-2 receptor binding domain (RBD) with soluble hACE2 receptor[19] waned with a
82 similar two-phase decay, dropping more rapidly before day 70 ($t_{1/2}$ = 238 days) and
83 slowing after day 70 ($t_{1/2}$ = 1912 days; Fig1C).
84
85 Plasma antibodies specific for SARS-CoV-2 S antigens (trimeric spike protein (S),
86 S1, S2 and RBD subdomains) and nucleocapsid (N) antigens were quantified
87 longitudinally using a multiplex bead array[25]. In contrast to neutralisation titres, decay
88 of S-specific IgG was best fit by a model of constant decay over the period of
89 observation ($t_{1/2}$ = 229 days), with rates of decay divergent for antibodies binding S1
90 ($t_{1/2}$ =115 days), S2 ($t_{1/2}$ = 344 days) and RBD antigens ($t_{1/2}$ = 126; Fig 1D, Extended

91 Data Fig. 2). Kinetics of decay were broadly consistent between IgG1 and IgG2
92 subclasses, with IgG3 displaying a more rapid, two phase decline (Extended Data Fig.
93 2). Consistent with a previous report[26], we find N-specific IgG decays significantly
94 more rapidly than S-specific IgG ($t_{1/2}$ = 71 and 229 days respectively, $p < 0.00001$,
95 Fig 1D). In contrast to IgG, S-specific IgM and IgA1 fit a two-phase decay, with a
96 more rapid early decay ($t_{1/2}$ = 55 and 42 days respectively) followed by a slower
97 decay in late convalescence ($t_{1/2}$ = 118 and >1000 days respectively; Fig 1D). A
98 comparison of decay rates between neutralising activity and antibody binding
99 demonstrated that early neutralisation decay occurs at a similar rate to the early
100 decline in S, RBD and S1-specific IgM (Fig 1E, Extended Data Fig 2). Neutralisation
101 titre at both early and late convalescence was well correlated with serum inhibition of
102 RBD-ACE2 binding and S, S1 and RBD specific IgG, IgM (and to a lesser extent
103 IgA1) responses, as well as with S2 and N specific IgG responses (Extended Data Fig
104 3). Neutralising activity during early convalescence was the best correlate of long-
105 term maintenance of neutralisation responses (Spearman rho=0.88, $p<0.00001$;
106 Extended Data Fig 3). Serum inhibition of RBD-ACE2 binding and S1-specific IgG
107 responses in early infection were also well correlated with neutralisation titre in late
108 convalescence (Spearman rho=0.79, 0.81, respectively; Extended Data Fig 3).
109 However, in a multiple regression model, once early neutralisation activity was
110 included no other significant predictors were identified ($p>0.15$ for all other
111 variables).
112
113 The decay of polyclonal antibody in plasma may obscure a more complex picture of
114 the dynamics of individual antibody specificities. To resolve longitudinal serological
115 decay at the level of a single clonotype, we adapted a novel mass spectrometry (MS)-

116 based quantitative proteomics workflow developed for serum autoantibody
117 profiling[27,28] to track unique CDR-H3 peptides matching recovered S-specific
118 immunoglobulins sequences from convalescent subjects[19] (n=4; Extended Data Fig
119 4A, B). Consistent with the decay of polyclonal S-specific antibody in the blood, we
120 find a decline in the relative abundance over time for each unique clonotype
121 (Extended Data Fig. 4C), although absolute rates of decay did vary, suggesting the
122 kinetics might to some degree be clonotype-, epitope- or subject-specific.
123
124 Anti-viral memory B and T cell responses will likely make additive contributions to
125 long-term immunological protection against COVID-19. SARS-CoV-2-specific B cell
126 responses were measured longitudinally in 31 subjects where sufficient cells were
127 available (Fig 1A) using flow cytometry and fluorescent S and RBD probes as
128 previously described[19]. Following infection, frequencies of IgG+ S-specific memory
129 B cells increased over time irrespective of disease severity (Fig. 2A and 2B; gating in
130 Supplementary Fig. S1). In contrast, S-specific IgA+ MBC frequencies remained
131 relatively stable while IgM+ MBC frequencies decreased (Fig. 2B). IgG+ S-specific
132 MBC remain significantly elevated at the final relative to the first available sampling
133 ($p<0.0001$), contrasting with stable IgA+ ($p=0.367$) and declining IgM+ populations
134 ($p<0.0001$) (Fig. 2C). Assessment of the activation status of S-specific IgG+ MBC
135 using CD21/CD27 staining[29] demonstrated decreased proportions of "activated" MBC
136 and a return to a resting (CD27+CD21+) phenotype over time (Extended Data Fig 5).
137 Although present at comparatively low frequencies, the dynamics of RBD-specific
138 MBC largely mirrored that of the parental S-specific population (Extended Data Fig
139 6). Modelling the growth rates reveals IgG+ S-specific MBC frequencies had a
140 doubling time of 48 days in early convalescence, after which point the doubling time

141 slowed to 843 days, with IgG+ RBD-specific cells MBC broadly comparable
142 (doubling time = 58 days early, $t_{1/2}$ = 247 days late) (Extended Data Fig 7). The
143 consistent and sustained increase in S-specific IgG+ MBC frequencies over time
144 aligns with a prior report of SARS-CoV-2 convalescent subjects[13], and with reports
145 from other viral infections[30] or replicating viral vaccines [31,326]. Given the relatively
146 low level of somatic mutation observed in S-specific antibodies recovered from
147 convalescent subjects to date[6,19] comparative studies at 6-9 months post-infection will
148 be informative to understand the maturation of the humoral response over time and
149 the protective potential of stably retained MBC populations.
150
151 Anti-viral memory T cell responses have been associated with amelioration of disease
152 for respiratory infection such as influenza[33]. S-specific cTFH and conventional CD4+
153 and CD8+ memory T cells (Tmem), were quantified using activation induced marker
154 (AIM) assays [19,22] (Methods) following stimulation with overlapping S (split into S1
155 or S2) peptide pools (Fig. 3A, 3B). Frequencies of S-specific memory T cells were
156 dynamic over time and varied between individuals, with evidence of either rapid
157 decline or stable maintenance (Fig. 3C). Pairwise comparison of cTFH or CD4+
158 Tmem frequencies at the final visit relative to the first available sampling
159 demonstrated a significant reduction in S-specific responses over time (p=0.0031 for
160 cTFH, p=0.0224 for CD4+ Tmem; Fig. 3D). In contrast, frequencies of S-specific
161 CD8+ Tmem were stable at a population level (p=0.3247), although individual
162 responses were varied (Fig. 3D). Modelling of the decay rates estimated $t_{1/2}$ of 128
163 days for cTFH (95% CI 67, 1247) and 119 days for CD4+ Tmem (95% CI 66, 612;
164 Extended Data Fig 8). In contrast, the estimated decay of CD8+ responses is not
165 significantly different from 0 ($t_{1/2}$ = 670 days, 95% CI 97, -136; Extended Data Fig 8).

166 Therefore, while we and others[34,35] find that CD4+ responses are generally higher
167 during early convalescence, CD8+ T cell responses appear relatively stable during late
168 convalescence.
169
170 Multiple studies have reported CCC cross-reactive CD4+ T cells in SARS-CoV-2
171 uninfected subjects, largely recognising epitopes in S2[22,35,36]. To understand the
172 influence that recall of pre-existing CCC cross-reactive immunity might have on
173 decay, we contrasted S1 and S2 responses among the CD4+ T cell subsets. For cTFH,
174 a significant drop in S1 responses was observed over time (p=0.0028), while S2
175 responses were comparably stable but did similarly trend downward (p=0.0657)
176 (Extended Data Fig 9A,B). Analogous patterns were observed for the CD4+ Tmem
177 cells (Extended Data Fig 9C,D). Consequently, S2-specific cTFH and CD4+ Tmem
178 populations predominated over S1-directed responses (p=0.0147 and p=0.0021
179 respectively) in late convalescence (Extended Data Fig 9B,D).
180
181 Polyclonal T cell responses to S comprise an array of immunodominant and
182 subdominant epitopes; we therefore additionally tracked single CD4+ T cell epitopes
183 in a subset of 9 donors (Extended Data Fig 10A). Strikingly, we observed substantial
184 inter- and intra-individual variability in longitudinal epitope-specific responses
185 (Extended Data Fig 10B,C); in some subjects, all epitope-specific responses tracked
186 similarly while in others distinct epitope-specific responses would vary independently
187 over time. In most, but not all, cases, peptide responses tracked similarly between the
188 cTFH and Tmem populations (Extended Data Fig 10C). Overall, some degree of T
189 cell immunity remains readily detectable in most subjects 4 months after infection,
190 although longitudinal epitope-specific frequencies were markedly less predictable.

191

192 Deconvoluting the protective potential of the suite of concomitant immune responses
193 elicited by SARS-CoV-2 infection is challenging. The general decline of serological
194 immunity over time (Fig 4A) was similarly observed for most memory immune cell
195 subsets except for IgG+ and IgA+ MBC populations (Fig 4B). Importantly, rates of
196 immune decay are likely to stabilise over time to levels of homeostatic maintenance[37],
197 although this set point is not yet clear for SARS-CoV-2. Neutralising antibody is the
198 most widely accepted protective correlate against a range of human respiratory
199 viruses[38]. However, any relationship between *in vitro* neutralisation titres and *in vivo*
200 protection for SARS-CoV-2 is unclear at present. We therefore developed a
201 simulation model (see Methods) employing the estimated initial distributions of
202 neutralisation titres and decay rates across subjects, to predict the time for titres to
203 drop below a nominated cut-off of 1:40, selected based on the 1:40 hemagglutination
204 inhibition titre (a surrogate for neutralisation activity) widely used as the 50%
205 protective titre for influenza[39]. Notably, 43% of our cohort were already below this
206 threshold in early convalescence, with 64% of subjects dropping below this threshold
207 in late convalescence. Simulating a population of 1000 individuals, and running the
208 model 1000 times, we find the median time for 50% of the population to drop below a
209 titre of 1:40 was 74 days (Fig 4C; 95% confidence interval 46 to >1000 days).
210 Assuming early neutralisation titres predicted titres into late convalescence, our
211 simulation also allows us to estimate how higher initial levels of neutralisation may
212 affect the proportion of individuals maintaining titres above 1:40. We found that if
213 aiming for a median of 50% of individuals with a titre above 1:40 at one year, initial
214 neutralisation titres at about day 30 would need to be in the order of 2.1-fold higher
215 than that observed in our convalescent cohort (95% CI = no increase to 16.9-fold

216 increase required). It is important to emphasise that at present the in vitro
217 neutralisation titre required and the additive contribution of other immune responses
218 to protective immunity are unknown. In addition, our analysis assumes that immunity
219 to vaccination decays at a similar rate to infection, and that the decay of neutralisation
220 titre from day 70 to around 140 predicts immune decay over the first year. Despite the
221 limitations inherent in these assumptions, this analysis provides an approach to
222 estimating the target level of immune response necessary for effective vaccination.
223
224 Overall, we find that both neutralising and binding antibody responses decay as
225 expected after recovery from COVID-19, assessed using polyclonal assays and at the
226 level of single clonotypes. While incredibly durable protective antibody responses
227 have been reported for other viral infections such as measles and smallpox[4], our data
228 suggests that SARS-CoV-2 is more likely to mirror immunity to endemic CCC, where
229 serum antibody responses decline with a likelihood of increasing susceptibility to
230 homologous virus within 1-2 years[5]. Neutralising antibody is a presumed but not yet
231 proven correlate of immune protection for SARS-CoV-2. Assuming similar immune
232 kinetics, our modelling suggests SARS-CoV-2 vaccines would likely need to elicit
233 substantially more potent neutralising titres than infection to induce durable
234 protection. Encouragingly, many early vaccine candidates have exceeded this metric
235 when compared against sera from convalescent subjects in clinical trials reported to
236 date[40,41]. Persistence of serum antibody is unlikely to be the sole determinant of long-
237 lasting immunity, with anamnestic recall of stably maintained memory T and B cell
238 populations likely reducing infection or disease. The magnitude, quality and
239 protective potential of cellular responses against SARS-CoV-2 requires further
240 definition. Although T cell memory in the blood contracts several months post

241 infection, a rise in S-specific IgG+ memory B cells to a median level of ~0.8% of all
242 IgG+ memory B cells by 4 months suggests even mild-moderate COVID-19 induces
243 substantial cellular immune memory.
244

245 **Materials and Methods**

246 **Ethics Statement**
247 The study protocols were approved by the University of Melbourne Human Research
248 Ethics Committee (#2056689) and the Southern Adelaide Clinical Human Research
249 Ethics Committee (#39.034), and all associated procedures were carried out in
250 accordance with the approved guidelines. All participants provided written informed
251 consent in accordance with the Declaration of Helsinki.

252 **Subject recruitment and sample collection**
253 Subjects who had recovered from COVID-19 were recruited through contacts with the
254 investigators and invited to provide serial blood samples. Subject characteristics of
255 SARS-CoV-2 convalescent subjects are collated in Extended Data Fig 1. For all
256 participants, whole blood was collected with sodium heparin anticoagulant. Plasma
257 was collected and stored at -80ºC, and PBMCs were isolated via Ficoll-Paque
258 separation, cryopreserved in 10% DMSO/FCS and stored in liquid nitrogen.
259

260 **Microneutralisation Assay**
261 SARS-CoV-2 isolate CoV/Australia/VIC01/2020 [42] was passaged in Vero cells and
262 stored at -80C. Plasma was heat-inactivated at 56°C for 30 min. Plasma was serially-
263 diluted 1:20 to 1:10240 before addition of 100 $TCID_{50}$ of SARS-CoV-2 in
264 MEM/0.5% BSA and incubation at room temperature for 1 hour. Residual virus
265 infectivity in the plasma/virus mixtures was assessed in quadruplicate wells of Vero

266 cells incubated in serum-free media containing 1 µg/ml TPCK trypsin at 37°C/5%
267 CO2; viral cytopathic effect was read on day 5. The neutralising antibody titre is
268 calculated using the Reed/Muench method as previously described[43,44]. All samples
269 were assessed in two independent microneutralisation assays.

270 **Expression of SARS-CoV-2 proteins**
271
272 A set of proteins was generated for serological and flow cytometric assays. The
273 ectodomain of SARS-CoV-2 (isolate WHU1;residues 1 – 1208) was synthesised with
274 furin cleavage site removed and P986/987 stabilisation mutations[45], a C-terminal T4
275 trimerisation domain, Avitag and His-tag, expressed in Expi293 cells and purified by
276 Ni-NTA affinity and size-exclusion chromatography using a Superose 6 16/70 column
277 (GE Healthcare). SARS-CoV S was biotinylated using Bir-A (Avidity). The SARS-
278 CoV-2 RBD[46] with a C-terminal His-tag (residues 319-541; kindly provided by
279 Florian Krammer) was similarly expressed and purified.
280

281 **SARS-CoV-2 bead-based multiplex assay**
282 The isotypes and subclasses of SARS-CoV-2 specific antibodies were detected as
283 previously described[25]. Briefly, a panel of SARS-CoV-2 antigens including trimeric
284 S, S1 (Sino Biological), S2 (ACROBiosystems), NP (ACROBiosystems,) and RBD[46]
285 were coupled to magnetic COOH- bioplex beads (Biorad) using a two-step
286 carbodiimide coupling reaction. 20µl of bead mixture containing 1000 beads per
287 region and 20µl of 1:200 diluted plasma were added per well. SARS-CoV-2- specific
288 antibodies were detected using phycoerythrin (PE)-conjugated mouse anti-human
289 pan-IgG, IgG1, IgG2, IgG3, IgA1 or IgA2 (Southern Biotech) at 1.3µg/ml, 25µl per
290 well. For the detection of IgM, biotinylated mouse anti-human IgM (mAb MT22;
291 MabTech) was added at 1.3µg/ml, 25µl per well followed by streptavidin-PE (SA-PE;

292 Thermo Fisher) at 1µg/ml. Plates were acquired by a FLEXMAP 3D (Luminex).
293 Median fluorescence intensity (MFI) for each isotype/subclass detector was assessed.
294 Background subtraction was conducted, removing background of blank (buffer only)
295 wells. Multiplex assays were repeated twice as two independent experiments.
296
297 **RBD-ACE2 binding inhibition multiplex bead-based assay**
298 RBD protein was coupled to bioplex beads (Biorad) as described above. 20µl of RBD
299 multiplex bead suspension containing 500 beads per well, 20µl of biotinylated
300 Avitag-ACE2 (kindly provided by Dale Godfrey and Nicholas Gherardin), final
301 concentration of 12.5µg/ml per well, along with 1:100 dilution of each subject's
302 plasma were added to 384 well plates. Plates were covered and incubated at room
303 temperature (RT) whilst shaking for 2 hours, and then washed twice with PBS
304 containing 0.05% Tween20 (PBST). Biotinylated Avitag-ACE2 was detected using
305 40µl per well of SA-PE at 4µg/ml, incubated with shaking for 1 hour at RT. 10µl of
306 PE-Biotin amplifier (Thermo Fisher) at 10µg/ml was added and incubated for 1 hour
307 with shaking at RT. Plates were washed and acquired on a FLEXMAP 3D (Luminex).
308 Anti-SARS-CoV-2 RBD neutralising human IgG1 antibody (ACROBiosystems,
309 USA) was included as a positive control, in addition to COVID-19 negative plasma
310 and buffer only negative controls. The MFI of bound ACE2 was measured after
311 background subtraction of no ACE2 controls. Maximal ACE2 binding MFI was
312 determined by buffer only controls. % ACE2 binding inhibition was calculated as
313 100% - (% ACE2 binding MFI per sample/ Maximal ACE2 binding). RBD-ACE2
314 binding inhibition multiplex assays were repeated independently twice.
315

316 **Flow cytometric detection of S- and RBD-specific memory B cells**

317 Probes for delineating SARS-CoV-2 S-specific B cells within cryopreserved human
318 PBMC were generated by sequential addition of streptavidin-PE (Thermofisher) to
319 trimeric S protein biotinylated using recombinant Bir-A (Avidity). SARS-CoV-2
320 RBD protein was directly labelled to APC using an APC Conjugation Lightning-link
321 kit (Abcam). Cells were stained with Aqua viability dye (Thermofisher). Monoclonal
322 antibodies for surface staining included: CD19-ECD (J3-119) (Beckman Coulter),
323 CD20 Alexa700 (2H7), IgM-BUV395 (G20-127), CD21-BUV737 (B-ly4), IgD-
324 Cy7PE (IA6-2), IgG-BV786 (G18-145) (BD), CD14-BV510 (M5E2), CD3-BV510
325 (OKT3), CD8a-BV510 (RPA-T8), CD16-BV510 (3G8), CD10-BV510 (HI10a),
326 CD27-BV605 (O323) (Biolegend), IgA-Vio450 (clone) (Miltenyi). Cells were
327 washed, fixed with 1% formaldehyde (Polysciences) and acquired on a BD
328 LSR Fortessa or BD Aria II.

329

330 **Flow cytometric detection of antigen-specific cTFH, memory CD4+ T cells and**
331 **memory CD8 T cells**

332 Cryopreserved human PBMC were thawed and rested for four hours at 37°C. Cells
333 were cultured in 96-well plates at $1x10^6$ cells/well and stimulated for 20 hours with
334 2µg/peptide/mL of peptide pools (15mer, overlapping by 11) covering the S1 or S2
335 domains of SARS-CoV-2. Selected donors were also stimulated with SEB (1µg/mL)
336 as a positive control, or individual peptides at 2ug/mL: NCTFEYVSQPFLMDL (S1
337 epitope; previously described in [47]); LPIGINITRFQTLLA (S1 epitope);
338 GWTFGAGAALQIPFA (S2 epitope); ALQIPFAMQMAYRFN (S2 epitope);
339 LLQYGSFCTQLNRAL (S2 epitope; [19,47]); QALNTLVKQLSSNFG (S2 epitope).
340 Following stimulation, cells were washed, stained with Live/dead Blue viability dye
341 (ThermoFisher), and a cocktail of monoclonal antibodies: CD27 BUV737 (L128),

342 CD45RA PeCy7 (HI100), CD20 BUV805 (2H7), (BD Biosciences), CD3 BV510
343 (SK7), CD4 BV605 (RPA-T4), CD8 BV650 (RPA-T8), CD25 APC (BC96), OX-40
344 PerCP-Cy5.5 (ACT35), CD69 FITC (FN50), CD137 BV421 (4B4-1) (Biolegend),
345 and CXCR5 PE (MU5UBEE, ThermoFisher). Cells were washed, fixed with 1%
346 formaldehyde and acquired on a BD LSR Fortessa using BD FACS Diva.
347
348 **Mass spectrometry (MS)-based quantitative proteomics of serum anti-S1**
349 **antibodies.** The workflow for anti-S1 proteomic profiling is shown in Extended Data
350 Figure 4A. Briefly, antibodies against SARS-CoV-2 S1 spike protein were affinity-
351 purified from convalescent plasma of COVID-19 subjects at different time points
352 using S1 protein-coupled magnetic beads (Acrobiosystems). IgG heavy chains were
353 isolated after reduced SDS-PAGE and digested with trypsin and chymotrypsin to
354 generate peptides for LC-MS/MS using a Thermo Scientific Orbitrap Exploris 480
355 mass spectrometer coupled to an Ultimate 3000 UHPLC (Dionex). De novo
356 sequencing data analysis was performed by Peaks studio X-plus software
357 (Bioinformatics Solution). Peptide sequences were referenced against recovered
358 heavy chain immunoglobulin sequences generated from single sorted S-specific
359 memory B cells[19] to identify matched CDR-H3 peptides. Anti-S1 clonotypic antibody
360 expression levels were monitored by parallel reaction monitoring (PRM) as described
361 previously[28,48]. Fragment ion extracted ion chromatograms (XICs) per CDR-H3
362 peptide were visualized in Skyline version 20.1.0.155 (University of Washington) and
363 inspected manually to ensure correct assignments. The annotated spectra of
364 individual peptides and their corresponding XICs are shown in Supplementary
365 Information.
366

367 **Estimating the decay rates**

368 We sought to predict the response variable (y_{ij} for patient i at timepoint j) as a
369 function of days post symptom onset, assay replicate (as a binary categorical variable)
370 and a random effect for each individual (both in in intercept and slope). The
371 dependency of the response variables on days post symptom onset can be modelled by
372 using one or two decay slopes. The model can be written as below:

373 $y_{ij} = \beta_0 + b_{0i} + \beta_1 R_{ij} + \beta_2 t_{ij} + b_{2i} t_{ij}$ – for a model with a single slope; and

374 $y_{ij} = \beta_0 + b_{0i} + \beta_1 R_{ij} + \beta_2 t_{ij} + b_{2i} t_{ij} + \beta_3 s_{ij} + b_{3i} s_{ij}$ – for a model with two
375 different slopes, in which:

376 $$s_{ij} = \begin{cases} 0, & t_{ij} < T_0 \\ t_{ij} - T_0, & t_{ij} \geq T_0. \end{cases}$$

377 The parameter β_0 is a constant (intercept), and b_{0i} is a patient-specific adjustment to
378 the overall intercept. The slope parameter β_2 is a fixed effect to capture the decay
379 slope before T_0; which also has a subject-specific random effect b_{2i}. To fit a model
380 with two different decay rates, an extra parameter β_3 (with a subject-specific random
381 effect b_{3i}) was added to represent the difference between the two slopes. Assay
382 variability between replicates was modelled as a single fixed effect β_1, in which we
383 coded the replicate as a binary categorical variable R_{ij}.

384 The response variables obtained were highly variable, containing zeros where the
385 value was below the limit of detection and contrasted with samples where very high
386 levels were observed. Thus, we performed log transformations of the non-zero data to
387 help normalize variability and censored every value less than 40 for the
388 microneutralisation data; every value less than 0.01 for the T cell and B cell data; and
389 every negative value for the multiplex data. More specifically, a mixed-effect
390 regression method that allows for censoring at the limit of detection was used to

391 estimate the parameters in the model. This was done by using *lmec* library in *R*, using
392 the ML algorithm to fit for the fixed effects[49]. We also tested if the decay of
393 serological response variables was fitted better by a single or two different decay
394 slopes (likelihood ratio test – based on the likelihood value and the difference in the
395 number of parameters). 95% CI for the fixed effect parameters was calculated based
396 on the standard error estimates, which can be obtained directly by using the *varFix*
397 function from *lmec* library. These analyses were carried out in *R* version 4.0.2.
398
399 **Simulating the decay of serological neutralisation activity**
400 To understand the decay in serum neutralisation we employed a simulation approach
401 using the parameters estimated from our mixed-effect censoring regression model of
402 decay. The fixed effect estimates averaged the intercept across experimental replicates
403 ($\beta_0 + \beta_{1/2}$ from equations above) and random effects were randomly selected from a
404 multivariate normal distribution with covariance matrix taken from the mixed-effect
405 regression with censoring lmec object. The residual error standard deviation for
406 simulated data every 10 days was taken from the lmec object. The confidence interval
407 for the percentage of subjects with a neutralisation titre above 1:40 was estimated
408 empirically with the percentile method by repeating the simulation 1000 times, where
409 for each replicate the fixed effects were drawn from a normal distribution based on
410 their standard error (as well as randomly selected random effects). To estimate the
411 fold increase in initial neutralisation titre required to achieve >50% of individuals
412 with a titre above 40 at 1 year we assumed that the rate of decay was constant from
413 day 70 onwards and projected forward the expected titres in the simulated
414 populations. The median and confidence intervals for the proportion of individuals
415 with titre > 40 were calculated from these 1000 simulated populations.

416 **Statistical Analyses**

417 Associations between neutralisation, inhibition of ACE2 binding and antibody
418 binding were assessed using both Spearman correlation, and multiple regression (R
419 version 4.0.2). The geometric mean of replicate neutralisation measurements and the
420 arithmetic mean of replicate measurements in other assays were used in the
421 correlation and regression analyses for other measurements. Neutralisation titres
422 below the limit of detection (a titre of 20) were assigned the arbitrary value 10 prior to
423 calculating the geometric mean for the purposes of the Spearman correlation, where
424 rank and not magnitude of the measurements is important. For the multiple regression
425 analysis values below the limit of detection were set at the detection threshold and
426 censoring regression was performed using the function *censReg (*from the *censReg*
427 library[50]) to determine which measurements during early convalescence were
428 significant predictors of neutralisation titre during late convalescence. Comparison of
429 B and T cell frequencies at first and final sampling was performed using Wilcoxon
430 Rank Sum test in GraphPad Prism 8. All statistical tests used were two sided.

431 **Competing interests**

432 The authors declare no competing interests.

433 **Data Availability**

434 All data are available from the corresponding author upon reasonable request.

435 **Code Availability**

436 All data analysis code can be made available on request.

437 **Authors' contributions**

438 A.K.W, J.A.J., J.J.W, H.-X.T., T.E.S., D.L.G., D.S.K., D.C., T.P.G, A.W.C., M.P.D.,
439 and S.J.K. designed the study and experiments. A.K.W., J.A.J., J.J.W., K.J.S, A.R.,
440 H.-X.T., W.S.L., K.M.W., H.G.K., R.E., S.K.D, H.E.K, F.L.M., T.E.S., and K.S.
441 performed experiments. A.K.W., J.A.J., J.J.W, H.-X.T., W.S.L., A.R., D.S.K., T.E.S.,

442 D.C., K.S., M.P.D., S.J.K. analysed the experimental data. A.K.W, J.A.J., J.J.W,
443 K.J.S, T.E.S., D.S.K., D.C., M.P.D., and S.J.K. wrote the manuscript. All authors
444 reviewed the manuscript.
445

446 **Acknowledgements**

447 We thank the generous participation of the trial subjects for providing samples. We
448 thank E. Haycroft, E. Lopez, C. Nelson and T. Amarasena and C. Batten (University
449 of Melbourne) for excellent technical assistance. The SARS-CoV-2 RBD expression
450 plasmids were kindly provided by F. Krammer (Icahn School of Medicine at Mt
451 Sinai). Recombinant human ACE2 was kindly provided by N. Gherardin and D.
452 Godfrey (University of Melbourne). We acknowledge the Melbourne Cytometry
453 Platform (Melbourne Brain Centre node) for provision of flow cytometry services.
454 We thank T. Chataway and A. Colella (Flinders Proteomics Facility) for technical
455 support with quantitative proteomics. This study was supported by the Victorian
456 Government, an Australian government Medical Research Future Fund award
457 GNT2002073 (SJK, MPD, and AKW), the ARC Centre of Excellence in Convergent
458 Bio-Nano Science and Technology (SJK), an NHMRC program grant APP1149990
459 (SJK and MPD), NHMRC project grant GNT1162760 (AKW), an NHMRC-EU
460 collaborative award APP1115828 (SJK and MPD), the European Union Horizon 2020
461 Research and Innovation Programme under grant agreement 681137 (SJK), Emergent
462 Ventures Fast Grants (AWC), the Jack Ma Foundation (KS) and the A2 Milk
463 Company (KS). JAJ, DSK, and SJK are supported by NHMRC fellowships. JJW is
464 supported by Flinders University DVCR Fellowship and Flinders Health & Medical
465 Research Institute COVID-19 Research Grant. AKW, KS, DC and MPD are
466 supported by NHMRC Investigator grants. The Melbourne WHO Collaborating

467 Centre for Reference and Research on Influenza is supported by the Australian
468 Government Department of Health.
469

470 **Figure 1 – Dynamics of serological responses to SARS-CoV-2**

471 (**A**) Timeline of sample collection for each cohort participant (n=64 participants, 158
472 total samples). Samples included only in serological analysis are indicated in black
473 (n=33); samples included in both serological and cellular immune analysis are
474 indicated in red (n=31). Shaded areas indicate early (<50 days) and late (>100 days)
475 convalescent time periods, and dashed line indicates day 70 midpoint. **(B)**
476 Longitudinal microneutralisation endpoint titre and **(C)** inhibition of ACE2 binding
477 (%) for individuals. Best fit two-phase decay slope (red line) is indicated. **(D)**
478 Individual kinetics and best fit decay slopes for IgG binding to spike (S), IgG binding
479 to nucleoprotein (N), IgM binding to S and IgA1 binding to S. **(E)** Estimated half-life
480 and confidence intervals of the neutralising antibody titre before day70 (red) and after
481 day70 post-symptom onset (blue) are indicated as dashed vertical lines. Estimated
482 early decay rates and confidence intervals for serological inhibition of ACE2 and
483 antibody binding titres are indicated (single phase decay is shown in grey, two phase
484 decay indicated in red/blue).

485

486 **Figure 2 - Quantification of S-specific memory B cell responses.**

487 (**A**) Staining class-switched B cells (CD19+IgD-) with SARS-CoV-2 spike probes
488 allows the tracking of antigen-specific cells in subjects previously infected with
489 SARS-CoV-2. (**B**) Frequencies of S-specific IgG+, IgA+ or IgM+ memory B cells as
490 a proportion of CD19+CD20+IgD- B cells in PBMC samples were assessed
491 longitudinally (n=31 subjects). (**C**) Comparison of S-specific IgG+, IgA+ or IgM+
492 memory B cell frequencies at the earliest and latest timepoint available for each
493 individual (n=31). Statistics assessed by two-tailed Wilcoxon test.

494

495 **Figure 3 - Quantification of antigen-specific CD4+ and CD8+ T cell responses.**
496 (**A**) Representative staining of AIM markers (CD25, OX-40) on CD4+ Tmem cells
497 (CD3+CD4+CD8-CD45RA-CXCR5-) after stimulation with vehicle, S1 or S2 peptide
498 pools in longitudinal samples from 1 participant (top row, day 33; middle row, day
499 61; bottom row, day 143). (**B**) Representative staining of AIM markers (CD69,
500 CD137) on CD8+ Tmem cells (CD3+CD8+CD4-non-naïve) in longitudinal samples
501 from 1 participant (top row, day 41; middle row, day 85; bottom row, day 120). (**C**)
502 Longitudinal changes in the frequency of total S (S1+S2 pool responses after
503 background subtraction)-specific responses among cTFH, CD4+ and CD8+ Tmem
504 subsets (n=31). (**D**) Comparison of S-specific T cell responses at the earliest and latest
505 timepoint available for each individual (n=31). Statistics assessed by two-tailed
506 Wilcoxon test.
507
508 **Figure 4 – Modelling of concomitant immune responses after COVID-19**
509 (**A**) Rates of decay of serological neutralisation activity, ACE2 binding inhibition, and
510 S-specific IgG, IgM and IgA following recovery from SAR-CoV-2 infection. (**B**)
511 Fitted Growth and decay rates for S-specific memory T cell and B cell frequencies in
512 PBMC. (**C**) Simulation of elicitation and decay of serological neutralisation activity in
513 1000 individuals based on distributions observed in our SARS-CoV-2 convalescent
514 cohort. The simulation was repeated 1000 times to estimate the proportion of
515 individuals maintaining a neutralisation titre above 1:40 across multiple simulations
516 (median and 95% confidence intervals shown in red).
517
518 **Extended data figure 1. Demographic and clinical characteristics of the**
519 **convalescent COVID-19 cohort.**

520

521 **Extended data figure 2: Fitting of the decline in antibody binding across**

522 **different immunoglobulin isotypes**.

523 The best-fit model and half-lives are shown for the fitting of the decay of antibody

524 binding to different SARS-CoV-2 antigens (n=64 subjects). Two-phase decay is

525 indicated by red (before day 70) and blue (after day 70) shaded areas. No shading

526 indicates where single-phase decay provided the best fit.

527

528 **Extended Data Figure 3: Correlation of antibody binding and ACE2 inhibition**

529 **with neutralisation.**

530 A heat-map of Spearman correlations between neutralisation titre and the serological

531 measurements of antibody binding (by isotype and antigen). Correlations were

532 assessed in early (≤50 days, left column n=54 subjects) and late (≥100 days, right

533 middle column, n=47 subjects) convalescence in all subjects were data was available.

534 The association between early antibody binding and late neutralisation is also shown

535 (right column, n=47 subjects). All correlations are Spearman correlations. *P≤0.05,

536 **P≤0.01, ***P≤0.001.

537

538 **Extended Data Figure 4: MS-based quantification of immunoprecipitated S1-**

539 **specific clonotypic antibodies.**

540 **(A)** Combined B cell receptor sequencing and proteomics platform enables

541 identification and quantification of circulating anti-S1 antibodies. S1-specific IgG was

542 purified from plasma of SARS-CoV-2 convalescent subjects using antigen-coupled

543 magnetic beads and heavy chains subject to LC-MC/MS. Peptide spectra are searched

544 against B-cell receptor sequencers recovered from single sorted S-specific memory B
545 cells from the same individuals to identify clonotypes based upon CDR-H3 amino
546 acid sequence. Clonotype specific peptides are then used as barcodes for relative
547 quantitative parallel reaction monitoring (PRM) for tracking in longitudinal plasma
548 samples. Targeted peptides are monitored during elution from HPLC and individual
549 peptides quantified based on abundance chromatography curves. **(B)** Clonotypes
550 identified based on matched CDR-H3 sequences from S1-specific plasma IgG and B
551 cell receptor sequences from SARS-CoV-2 convalescent subjects (n=4). **(C)**
552 Longitudinal changes in the relative plasma abundance of anti-S1 clonotypes within
553 four convalescent subjects over time. The quantity of each reference peptide is
554 expressed as area under the curve (AUC) derived from extracted ion chromatography.

555

556 **Extended Data Figure 5: Activation status of S-specific IgG+ memory B cells.**
557 **(A)** Memory B cell phenotypes identified by CD21 and CD27 co-staining of S+
558 CD19+CD20+IgD-IgG+ B cells (red) overlaid onto parental CD19+CD20+IgD-IgG+
559 B cells (black) and **(B)** the corresponding frequencies of "activated" (CD27+CD21-)
560 or resting (CD27+CD21+) in in PBMC samples were assessed longitudinally (n=31
561 subjects).

562

563 **Extended Data Figure 6: RBD-specific memory B cell dynamics.**
564 **(A)** Frequencies of RBD-specific IgG+, IgA+ or IgM+ memory B cells as a
565 proportion of CD19+CD20+IgD- B cells in PBMC samples were assessed
566 longitudinally. **(B)** Comparison of RBD-specific IgG+, IgA+ or IgM+ memory B cell
567 frequencies at the earliest and latest timepoint available for each individual (n=31).
568 Statistics assessed by two-tailed Wilcoxon test.

569

570 **Extended Data Figure 7: Fitting of the kinetics of S- and RBD-specific memory B**
571 **cell responses over time.**
572 The best-fit half-lives are shown for the fitting of the growth and/or decay of S- or
573 RBD-specific memory B cells (n=31 subjects). Two-phase decay is indicated by red
574 (before day 70) and blue (after day 70) shaded areas. No shading indicates where a
575 single-phase decay model was used to fit the data.
576

577 **Extended Data Figure 8: Fitting of the decline in SARS-CoV-2-specific T cells**
578 **over time.**
579 The best-fit half-lives are shown for the fitting of the decay of cTFH, CD4+ Tmem
580 and CD8+ Tmem specific to total S (S1+S2 responses combined), S1 or S2 peptide
581 pools (n=31 subjects). In all cases decay was fit with a single-phase decay model with
582 the half-lives shown.
583

584 **Extended Data Figure 9: S1 and S2-specific CD4+ T cell responses.**
585 **(A, C)** Representative staining of AIM markers following S1 and S2 peptide pool
586 stimulation among **(A)** cTFH (CD3+CD4+CD8-CD45RA-CXCR5+) or **(C)** CD4+
587 Tmem cells and longitudinal cohort analysis (n=31). **(B, D)** Comparison of S1 or S2-
588 specific **(B)** cTFH or **(D)** CD4+ Tmem responses at the earliest and latest visit for
589 each participant, as well as paired frequency of S1 versus S2 responses at the initial or
590 final visit (n=31). Statistics assessed by two-tailed Wilcoxon test.
591

592 **Extended Data Figure 10: Epitope-specific CD4+ T cell responses.**

593 **(A)** Representative staining of AIM markers following S1 or S2 peptide pool or

594 individual peptide stimulation among the CD4+ Tmem population. **(B,C)**

595 Longitudinal peptide-specific frequencies in individual subjects (n=9; solid line,

596 CD4+ Tmem; dashed line, cTFH) for whom **(B)** multiple or **(C)** single epitopes were

597 identified.

598 **References**

599 1. Deng, W., *et al.* Primary exposure to SARS-CoV-2 protects against reinfection
600 in rhesus macaques. *Science (New York, N.Y.)* **369**, 818-823 (2020).
601 2. Chandrashekar, A., *et al.* SARS-CoV-2 infection protects against rechallenge
602 in rhesus macaques. *Science (New York, N.Y.)* **369**, 812-817 (2020).
603 3. To, K.K., *et al.* COVID-19 re-infection by a phylogenetically distinct SARS-
604 coronavirus-2 strain confirmed by whole genome sequencing. *Clinical*
605 *infectious diseases : an official publication of the Infectious Diseases Society*
606 *of America* (2020).
607 4. Amanna, I.J., Carlson, N.E. & Slifka, M.K. Duration of humoral immunity to
608 common viral and vaccine antigens. *The New England journal of medicine*
609 **357**, 1903-1915 (2007).
610 5. Edridge, A.W., *et al.* Coronavirus protective immunity is short-lasting.
611 *medRxiv*, 2020.2005.2011.20086439 (2020).
612 6. Robbiani, D.F., *et al.* Convergent antibody responses to SARS-CoV-2 in
613 convalescent individuals. *Nature* (2020).
614 7. Ibarrondo, F.J., *et al.* Rapid Decay of Anti-SARS-CoV-2 Antibodies in
615 Persons with Mild Covid-19. *The New England journal of medicine* (2020).
616 8. Crawford, K.H., *et al.* Dynamics of neutralizing antibody titers in the months
617 after SARS-CoV-2 infection. *medRxiv*, 2020.2008.2006.20169367 (2020).
618 9. Isho, B., *et al.* Mucosal versus systemic antibody responses to SARS-CoV-2
619 antigens in COVID-19 patients. *medRxiv*, 2020.2008.2001.20166553 (2020).
620 10. Yao, X.-Y., *et al.* Neutralizing and binding antibody kinetics of COVID-19
621 patients during hospital and convalescent phases. *medRxiv*,
622 2020.2007.2018.20156810 (2020).
623 11. Wu, J., *et al.* SARS-CoV-2 infection induces sustained humoral immune
624 responses in convalescent patients following symptomatic COVID-19.
625 *medRxiv*, 2020.2007.2021.20159178 (2020).
626 12. Beaudoin-Bussières, G., *et al.* Decline of humoral responses against SARS-
627 CoV-2 Spike in convalescent individuals. *bioRxiv*, 2020.2007.2009.194639
628 (2020).
629 13. Rodda, L.B., *et al.* Functional SARS-CoV-2-specific immune memory persists
630 after mild COVID-19. *medRxiv*, 2020.2008.2011.20171843 (2020).
631 14. Seow, J., *et al.* Longitudinal evaluation and decline of antibody responses in
632 SARS-CoV-2 infection. *medRxiv*, 2020.2007.2009.20148429 (2020).
633 15. Muecksch, F., *et al.* Longitudinal analysis of clinical serology assay
634 performance and neutralising antibody levels in COVID19 convalescents.
635 *medRxiv*, 2020.2008.2005.20169128 (2020).
636 16. Wajnberg, A., *et al.* SARS-CoV-2 infection induces robust, neutralizing
637 antibody responses that are stable for at least three months. *medRxiv*,
638 2020.2007.2014.20151126 (2020).
639 17. Brochot, E., *et al.* Anti-Spike, anti-Nucleocapsid and neutralizing antibodies in
640 SARS-CoV-2 inpatients and asymptomatic carriers. *medRxiv*,
641 2020.2005.2012.20098236 (2020).
642 18. Seydoux, E., *et al.* Analysis of a SARS-CoV-2-Infected Individual Reveals
643 Development of Potent Neutralizing Antibodies with Limited Somatic
644 Mutation. *Immunity* **53**, 98-105.e105 (2020).
645 19. Juno, J.A., *et al.* Humoral and circulating follicular helper T cell responses in
646 recovered patients with COVID-19. *Nature medicine* (2020).

20. Schulien, I., *et al.* Ex vivo detection of SARS-CoV-2-specific CD8+ T cells: rapid induction, prolonged contraction, and formation of functional memory. *bioRxiv*, 2020.2008.2013.249433 (2020).
21. Neidleman, J., *et al.* SARS-CoV-2-specific T cells exhibit phenotypic features of robust helper function, lack of terminal differentiation, and high proliferative potential. *Cell Rep Med*, 100081 (2020).
22. Grifoni, A., *et al.* Targets of T Cell Responses to SARS-CoV-2 Coronavirus in Humans with COVID-19 Disease and Unexposed Individuals. *Cell* **181**, 1489-1501.e1415 (2020).
23. Braun, J., *et al.* SARS-CoV-2-reactive T cells in healthy donors and patients with COVID-19. *Nature* (2020).
24. Habel, J.R., *et al.* Suboptimal SARS-CoV-2-specific CD8+ T-cell response associated with the prominent HLA-A*02:01 phenotype. *medRxiv*, 2020.2008.2017.20176370 (2020).
25. Selva, K.J., *et al.* Distinct systems serology features in children, elderly and COVID patients. *medRxiv*, 2020.2005.2011.20098459 (2020).
26. Grandjean, L., *et al.* Humoral Response Dynamics Following Infection with SARS-CoV-2. *medRxiv*, 2020.2007.2016.20155663 (2020).
27. Singh, M., *et al.* Lymphoma Driver Mutations in the Pathogenic Evolution of an Iconic Human Autoantibody. *Cell* **180**, 878-894.e819 (2020).
28. Wang, J.J., *et al.* Molecular Profiling and Clonal Tracking of Secreted Rheumatoid Factors in Primary Sjögren's Syndrome. *Arthritis & rheumatology (Hoboken, N.J.)* **70**, 1617-1625 (2018).
29. Lau, D., *et al.* Low CD21 expression defines a population of recent germinal center graduates primed for plasma cell differentiation. *Science immunology* **2**(2017).
30. Davis, C.W., *et al.* Longitudinal Analysis of the Human B Cell Response to Ebola Virus Infection. *Cell* **177**, 1566-1582.e1517 (2019).
31. Matsuda, K., *et al.* Prolonged evolution of the memory B cell response induced by a replicating adenovirus-influenza H5 vaccine. *Science immunology* **4**(2019).
32. Wec, A.Z., *et al.* Longitudinal dynamics of the human B cell response to the yellow fever 17D vaccine. *Proceedings of the National Academy of Sciences of the United States of America* **117**, 6675-6685 (2020).
33. Brown, D.M., Dilzer, A.M., Meents, D.L. & Swain, S.L. CD4 T cell-mediated protection from lethal influenza: perforin and antibody-mediated mechanisms give a one-two punch. *Journal of immunology (Baltimore, Md. : 1950)* **177**, 2888-2898 (2006).
34. Grifoni, A., *et al.* Targets of T Cell Responses to SARS-CoV-2 Coronavirus in Humans with COVID-19 Disease and Unexposed Individuals. *Cell* (2020).
35. Weiskopf, D., *et al.* Phenotype and kinetics of SARS-CoV-2-specific T cells in COVID-19 patients with acute respiratory distress syndrome. *Science immunology* **5**(2020).
36. Mateus, J., *et al.* Selective and cross-reactive SARS-CoV-2 T cell epitopes in unexposed humans. *Science (New York, N.Y.)* (2020).
37. Crotty, S., *et al.* Cutting edge: long-term B cell memory in humans after smallpox vaccination. *Journal of immunology (Baltimore, Md. : 1950)* **171**, 4969-4973 (2003).
38. Plotkin, S.A. Updates on immunologic correlates of vaccine-induced protection. *Vaccine* **38**, 2250-2257 (2020).

39. Cox, R.J. Correlates of protection to influenza virus, where do we go from here? *Human vaccines & immunotherapeutics* **9**, 405-408 (2013).
40. Keech, C., *et al.* Phase 1-2 Trial of a SARS-CoV-2 Recombinant Spike Protein Nanoparticle Vaccine. *The New England journal of medicine* (2020).
41. Jackson, L.A., *et al.* An mRNA Vaccine against SARS-CoV-2 - Preliminary Report. *The New England journal of medicine* (2020).
42. Caly, L., *et al.* Isolation and rapid sharing of the 2019 novel coronavirus (SARS-CoV-2) from the first patient diagnosed with COVID-19 in Australia. *Med J Aust* **212**, 459-462 (2020).
43. Houser, K.V., *et al.* Prophylaxis With a Middle East Respiratory Syndrome Coronavirus (MERS-CoV)-Specific Human Monoclonal Antibody Protects Rabbits From MERS-CoV Infection. *The Journal of infectious diseases* **213**, 1557-1561 (2016).
44. Subbarao, K., *et al.* Prior infection and passive transfer of neutralizing antibody prevent replication of severe acute respiratory syndrome coronavirus in the respiratory tract of mice. *Journal of virology* **78**, 3572-3577 (2004).

Methods References:

45. Wrapp, D., *et al.* Cryo-EM structure of the 2019-nCoV spike in the prefusion conformation. *Science (New York, N.Y.)* **367**, 1260-1263 (2020).
46. Amanat, F., *et al.* A serological assay to detect SARS-CoV-2 seroconversion in humans. *Nature medicine* (2020).
47. Peng, Y., *et al.* Broad and strong memory CD4+ and CD8+ T cells induced by SARS-CoV-2 in UK convalescent individuals following COVID-19. *Nature immunology* (2020).
48. Wang, J.J., Colella, A.D., Beroukas, D., Chataway, T.K. & Gordon, T.P. Precipitating anti-dsDNA peptide repertoires in lupus. *Clinical and experimental immunology* **194**, 273-282 (2018).
49. Vaida, F. & Liu, L. Fast Implementation for Normal Mixed Effects Models With Censored Response. *J Comput Graph Stat* **18**, 797-817 (2009).
50. Henningsen, A. censReg: Censored Regression (Tobit) Models. (2017).

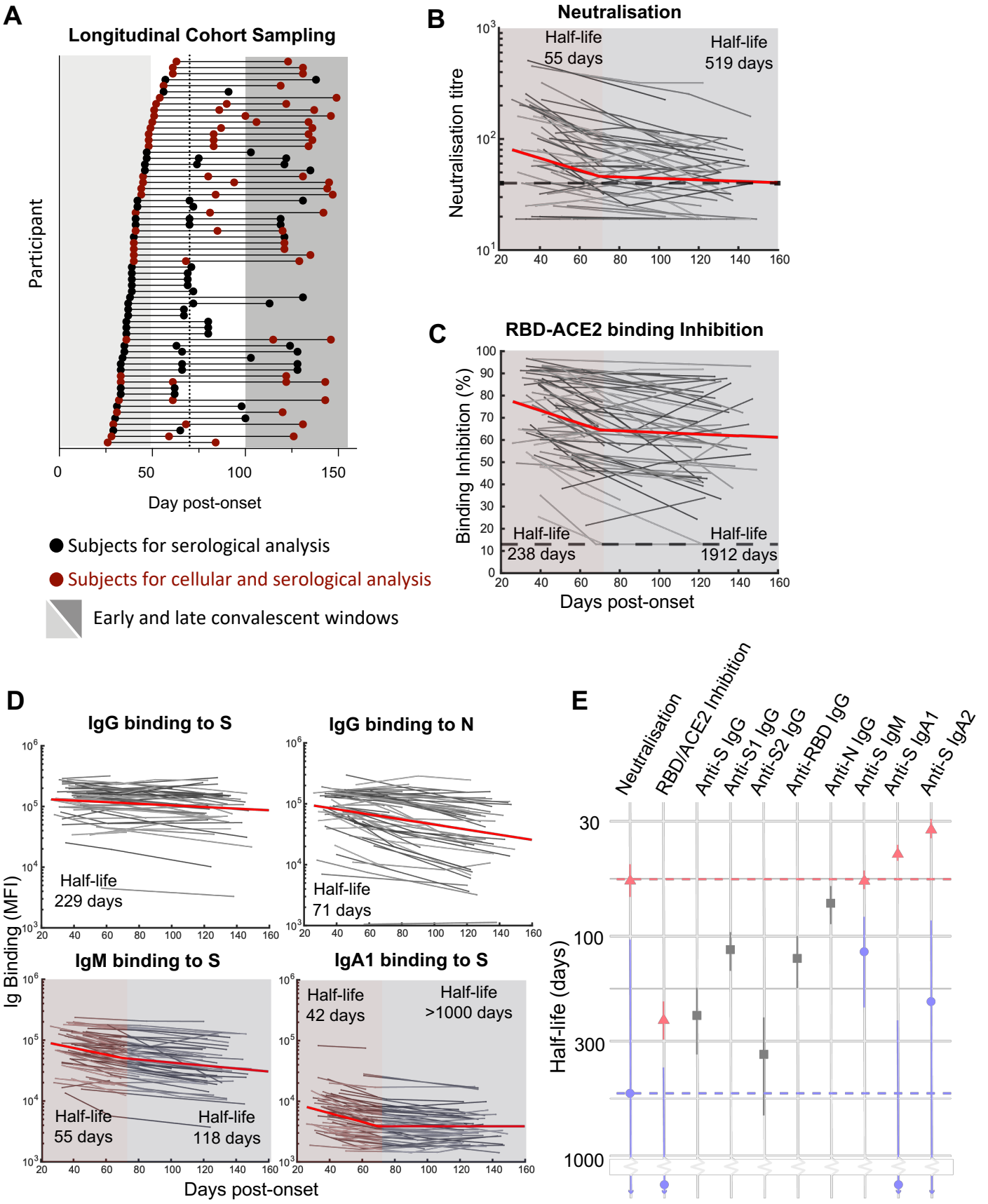
A
Longitudinal Cohort Sampling
Participant
0
50
100
150
Day post-onset
Subjects for serological analysis
Subjects for cellular and serological analysis
Early and late convalescent windows
B
Neutralisation
Neutralisation titre
Half-life
55 days
Half-life
519 days
C
RBD-ACE2 binding Inhibition
Binding Inhibition (%)
Half-life
238 days
Half-life
1912 days
Days post-onset
D
IgG binding to S
IgG binding to N
IgM binding to S
IgA1 binding to S
Ig Binding (MFI)
Half-life
229 days
Half-life
71 days
Half-life
55 days
Half-life
118 days
Half-life
42 days
Half-life
>1000 days
Days post-onset
E
Neutralisation
RBD/ACE2 Inhibition
Anti-S IgG
Anti-S1 IgG
Anti-S2 IgG
Anti-RBD IgG
Anti-N IgG
Anti-S IgM
Anti-S IgA1
Anti-S IgA2
Half-life (days)
30
100
300
1000

Figure 1 – Dynamics of serological responses to SARS-CoV-2

(**A**) Timeline of sample collection for each cohort participant (n=64 participants, 158 total samples). Samples included only in serological analysis are indicated in black (n=33); samples included in both serological and cellular immune analysis are indicated in red (n=31). Shaded areas indicate early (≤50 days) and late (≥100 days) convalescent time periods, and dashed line indicates day 70 midpoint. (**B**) Longitudinal microneutralisation endpoint titre and (**C**) inhibition of RBD-ACE2 binding (%) for individuals. Best fit two-phase decay slope (red line) is indicated. (**D**) Individual kinetics and best fit decay slopes for IgG binding to spike (S), IgG binding to nucleoprotein (N), IgM binding to S and IgA1 binding to S. (**E**) Estimated half-life and confidence intervals of the neutralising antibody titre before day70 (red) and after day70 post-symptom onset (blue) are indicated as dashed vertical lines. Estimated early decay rates and confidence intervals for serological inhibition of ACE2 and antibody binding titres are indicated (single phase decay is shown in grey, two phase decay indicated in red/blue).

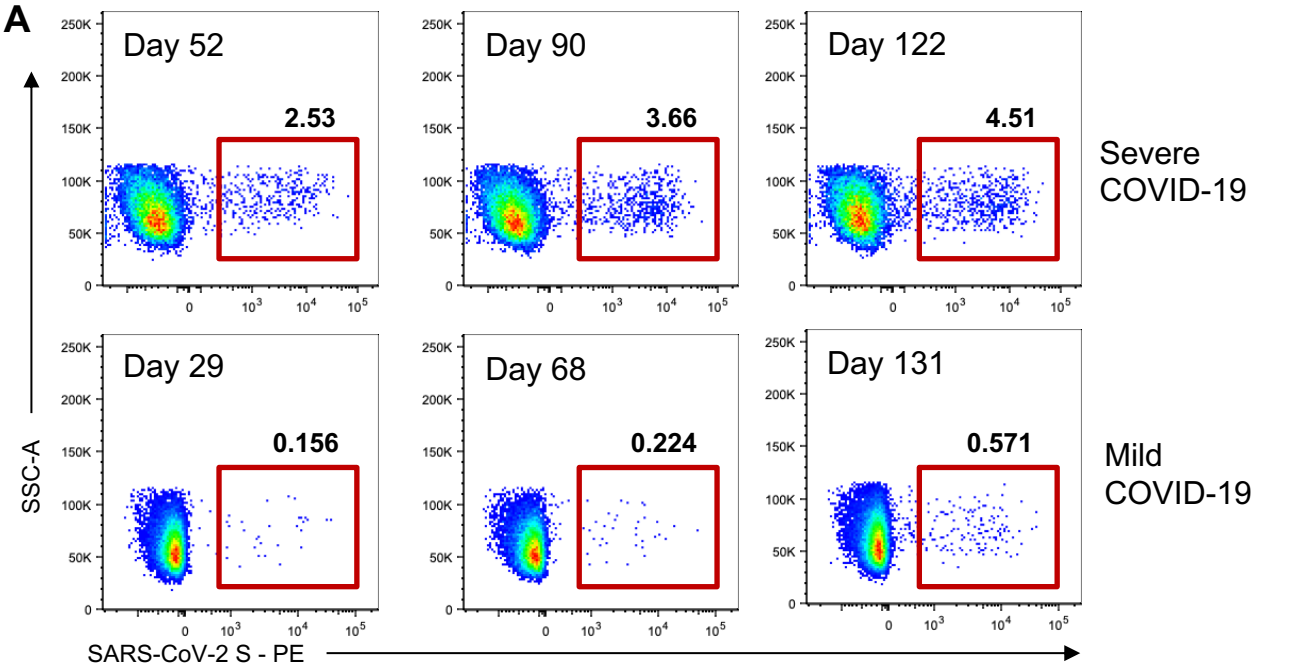
A
Day 52
2.53
Day 90
3.66
Day 122
4.51
Severe COVID-19
Day 29
0.156
Day 68
0.224
Day 131
0.571
Mild COVID-19
SSC-A
SARS-CoV-2 S - PE

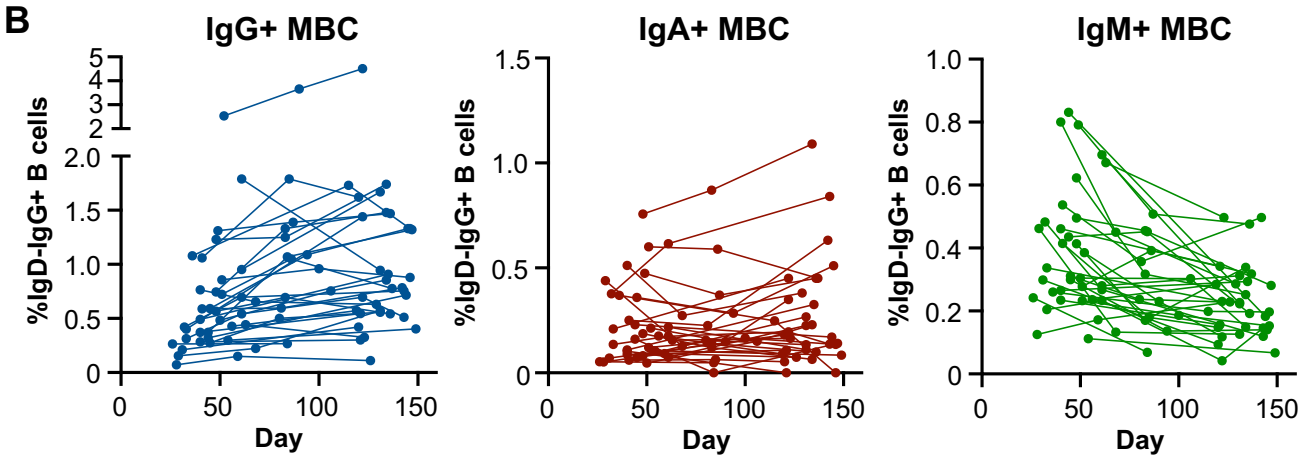
B
IgG+ MBC
IgA+ MBC
IgM+ MBC
%IgD-IgG+ B cells
Day

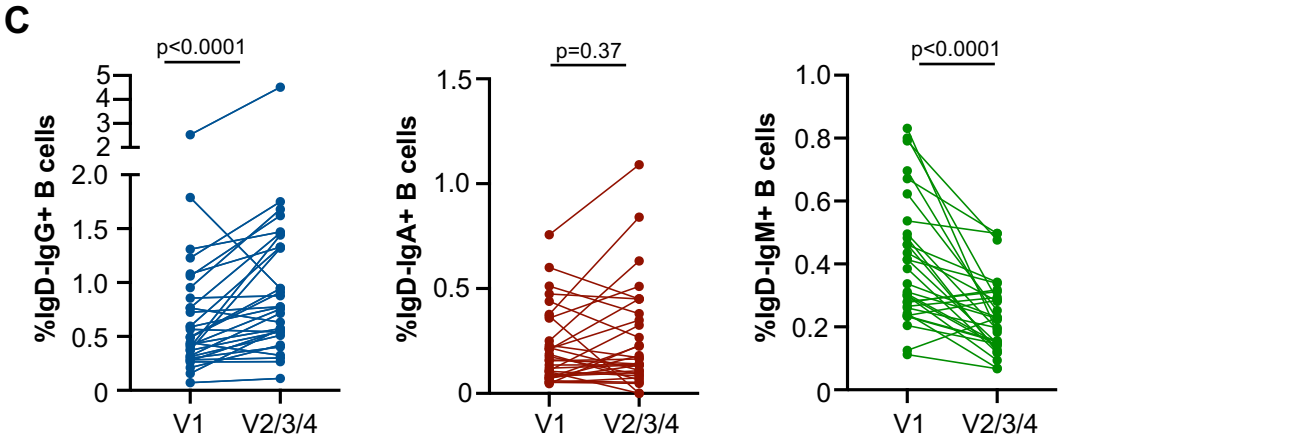
C
p<0.0001
p=0.37
p<0.0001
%IgD-IgG+ B cells
%IgD-IgA+ B cells
%IgD-IgM+ B cells
V1
V2/3/4

Figure 2 - Quantification of S-specific memory B cell responses.

(**A**) Staining class-switched B cells (CD19+IgD-) with SARS-CoV-2 spike probes allows the tracking of antigen-specific cells in subjects previously infected with SARS-CoV-2. (**B**) Frequencies of S-specific IgG+, IgA+ or IgM+ memory B cells as a proportion of CD19+CD20+IgD- B cells in PBMC samples were assessed longitudinally (n=31 subjects). (**C**) Comparison of S-specific IgG+, IgA+ or IgM+ memory B cell frequencies at the earliest and latest timepoint available for each individual (n=31). Statistics assessed by two-tailed Wilcoxon test.

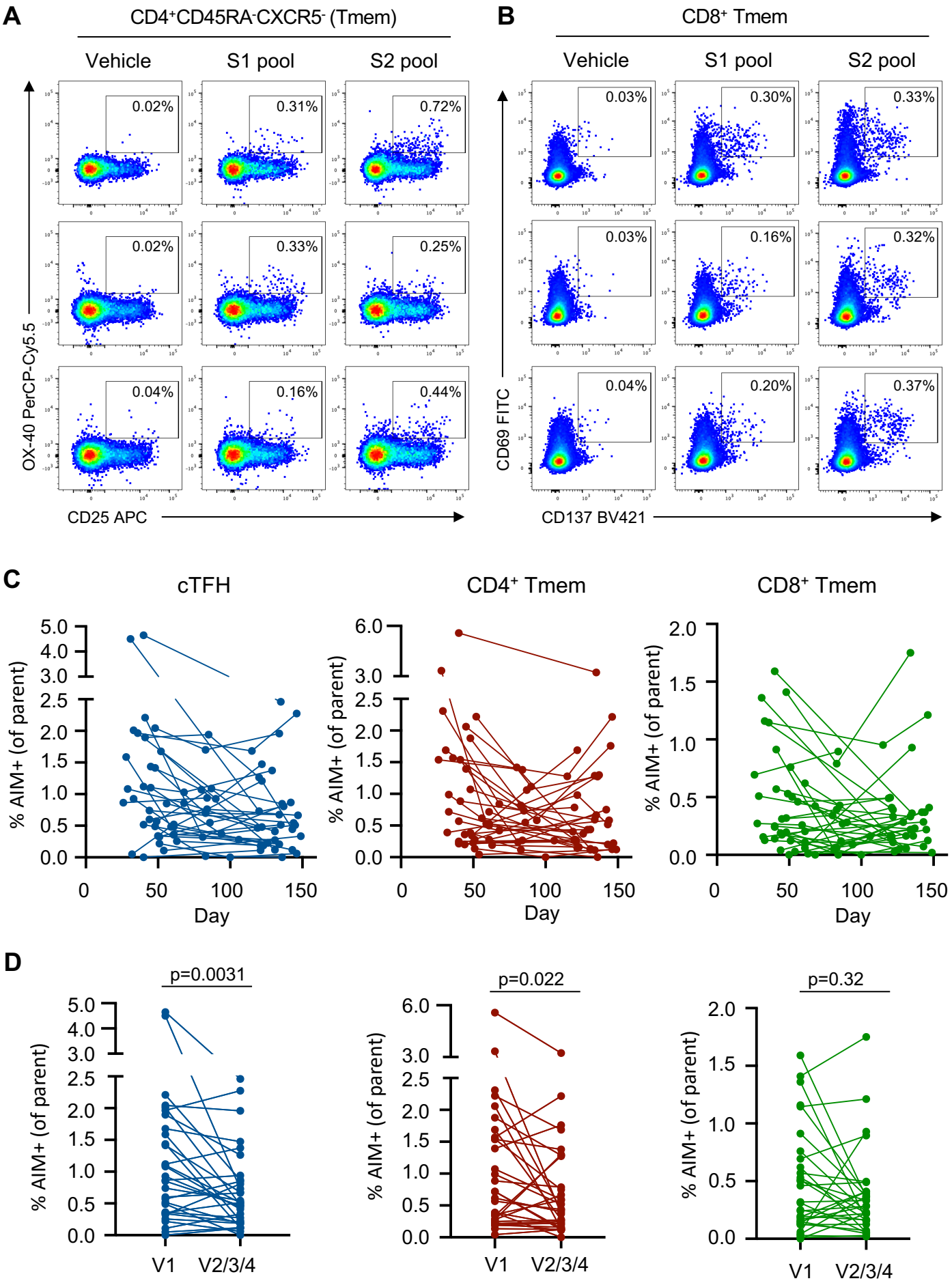
A
CD4+CD45RA-CXCR5- (Tmem)
Vehicle
S1 pool
S2 pool
0.02%
0.31%
0.72%
0.02%
0.33%
0.25%
0.04%
0.16%
0.44%
OX-40 PerCP-Cy5.5
CD25 APC
B
CD8+ Tmem
Vehicle
S1 pool
S2 pool
0.03%
0.30%
0.33%
0.03%
0.16%
0.32%
0.04%
0.20%
0.37%
CD69 FITC
CD137 BV421
C
cTFH
CD4+ Tmem
CD8+ Tmem
% AIM+ (of parent)
Day
D
p=0.0031
p=0.022
p=0.32
% AIM+ (of parent)
V1
V2/3/4

Figure 3 - Quantification of antigen-specific CD4+ and CD8+ T cell responses.

(**A**) Representative staining of AIM markers (CD25, OX-40) on CD4+ Tmem cells (CD3+CD4+CD8-CD45RA-CXCR5-) after stimulation with vehicle, S1 or S2 peptide pools in longitudinal samples from 1 participant (top row, day 33; middle row, day 61; bottom row, day 143). (**B**) Representative staining of AIM markers (CD69, CD137) on CD8+ Tmem cells (CD3+CD8+CD4-non-naïve) in longitudinal samples from 1 participant (top row, day 41; middle row, day 85; bottom row, day 120). (**C**) Longitudinal changes in the frequency of total S (S1+S2 pool responses after background subtraction)-specific responses among cTFH, CD4+ and CD8+ Tmem subsets (n=31). (**D**) Comparison of S-specific T cell responses at the earliest and latest timepoint available for each individual (n=31). Statistics assessed by two-tailed Wilcoxon test.

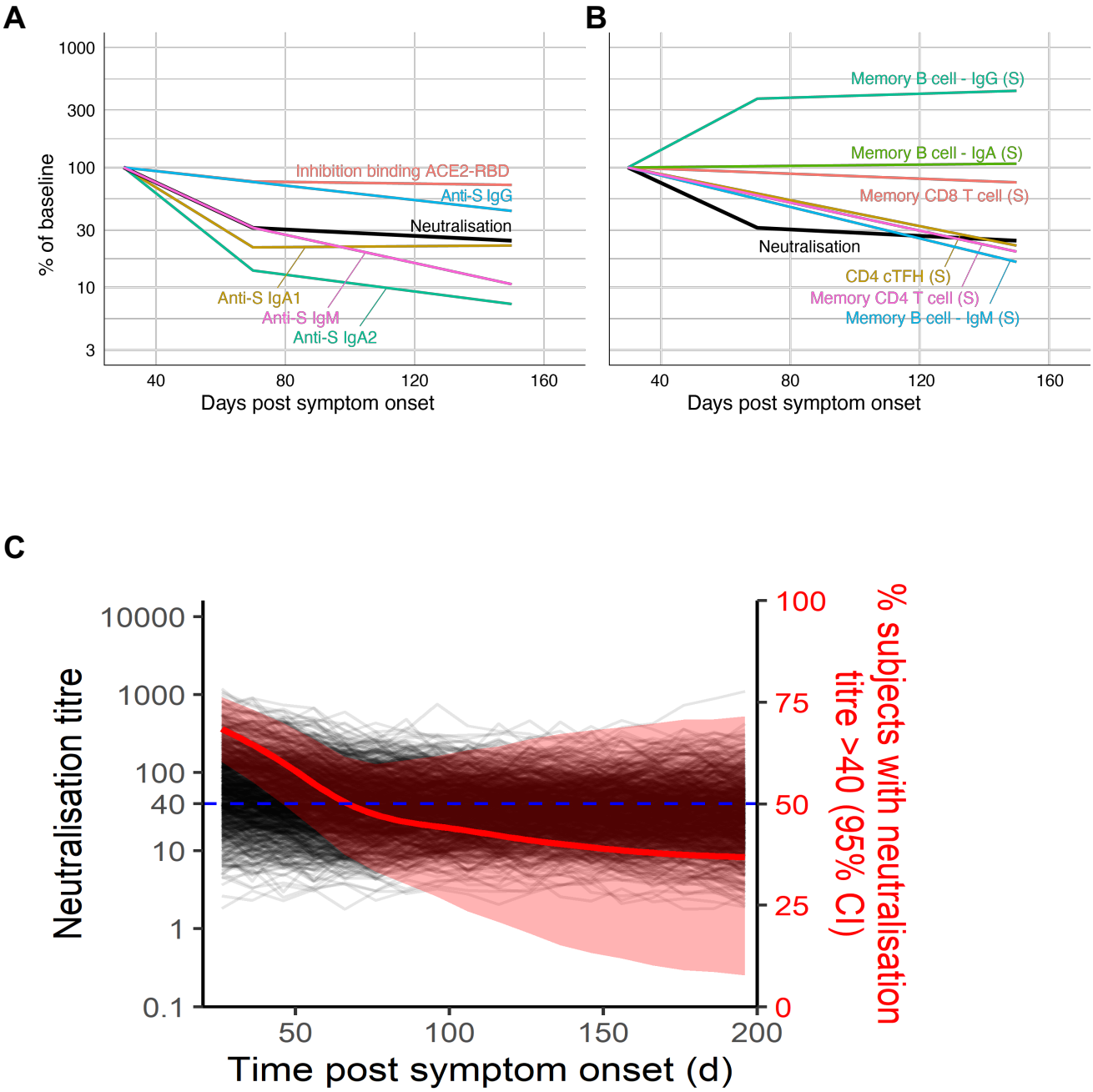
A
1000
300
100
30
10
3
% of baseline
Inhibition binding ACE2-RBD
Anti-S IgG
Neutralisation
Anti-S IgA1
Anti-S IgM
Anti-S IgA2
40
80
120
160
Days post symptom onset
B
Memory B cell - IgG (S)
Memory B cell - IgA (S)
Memory CD8 T cell (S)
Neutralisation
CD4 cTFH (S)
Memory CD4 T cell (S)
Memory B cell - IgM (S)
40
80
120
160
Days post symptom onset
C
10000
1000
100
40
10
1
0.1
Neutralisation titre
50
100
150
200
Time post symptom onset (d)
100
75
50
25
0
% subjects with neutralisation titre >40 (95% CI)

Figure 4 – Modelling of concomitant immune responses after COVID-19

(**A**) Rates of decay of serological neutralisation activity, ACE2 binding inhibition, and S-specific IgG, IgM and IgA following recovery from SAR-CoV-2 infection. (**B**) Fitted Growth and decay rates for S-specific memory T cell and B cell frequencies in PBMC. (**C**) Simulation of elicitation and decay of serological neutralisation activity in 1000 individuals based on distributions observed in our SARS-CoV-2 convalescent cohort. The simulation was repeated 1000 times to estimate the proportion of individuals maintaining a neutralisation titre above 1:40 across multiple simulations (median and 95% confidence intervals shown in red).

Extended Data Figures

	Full Cohort (n=64)	Cellular Analysis Cohort (n=31)
Age, median (IQR)	55 (62, 49)	52 (56, 31)
Gender, % female (n)	43.8% (28)	45.2% (14)
Disease severity, % (n) - mild	68.8% (44)	74.2% (23)
- moderate	23.4% (15)	16.1% (5)
- severe	7.8% (5)	9.7% (3)
Positive PCR test, % (n)	84.4% (54)	83.9% (26)

Extended data figure 1. Demographic and clinical characteristics of the convalescent COVID-19 cohort.

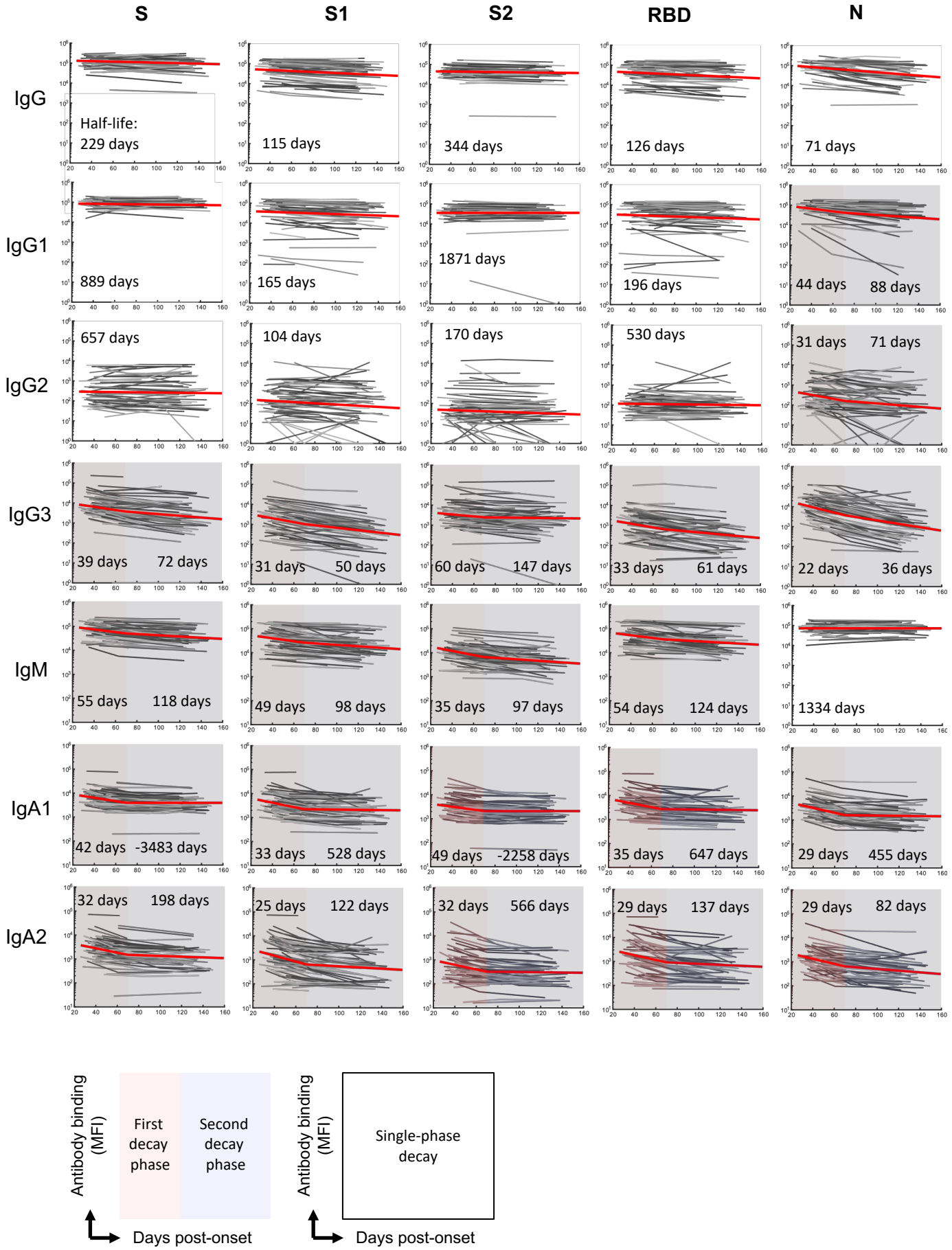
S
S1
S2
RBD
N
IgG
Half-life:
229 days
115 days
344 days
126 days
71 days
IgG1
889 days
165 days
1871 days
196 days
44 days
88 days
IgG2
657 days
104 days
170 days
530 days
31 days
71 days
IgG3
39 days
72 days
31 days
50 days
60 days
147 days
33 days
61 days
22 days
36 days
IgM
55 days
118 days
49 days
98 days
35 days
97 days
54 days
124 days
1334 days
IgA1
42 days
-3483 days
33 days
528 days
49 days
-2258 days
35 days
647 days
29 days
455 days
IgA2
32 days
198 days
25 days
122 days
32 days
566 days
29 days
137 days
29 days
82 days
Antibody binding (MFI)
First decay phase
Second decay phase
Days post-onset
Antibody binding (MFI)
Single-phase decay
Days post-onset

Extended data figure 2: Fitting of the decline in antibody binding across different immunoglobulin isotypes.

The best-fit model and half-lives are shown for the fitting of the decay of antibody binding to different SARS-CoV-2 antigens (n=64 subjects). Two-phase decay is indicated by red (before day 70) and blue (after day 70) shaded areas. No shading indicates where single-phase decay provided the best fit.

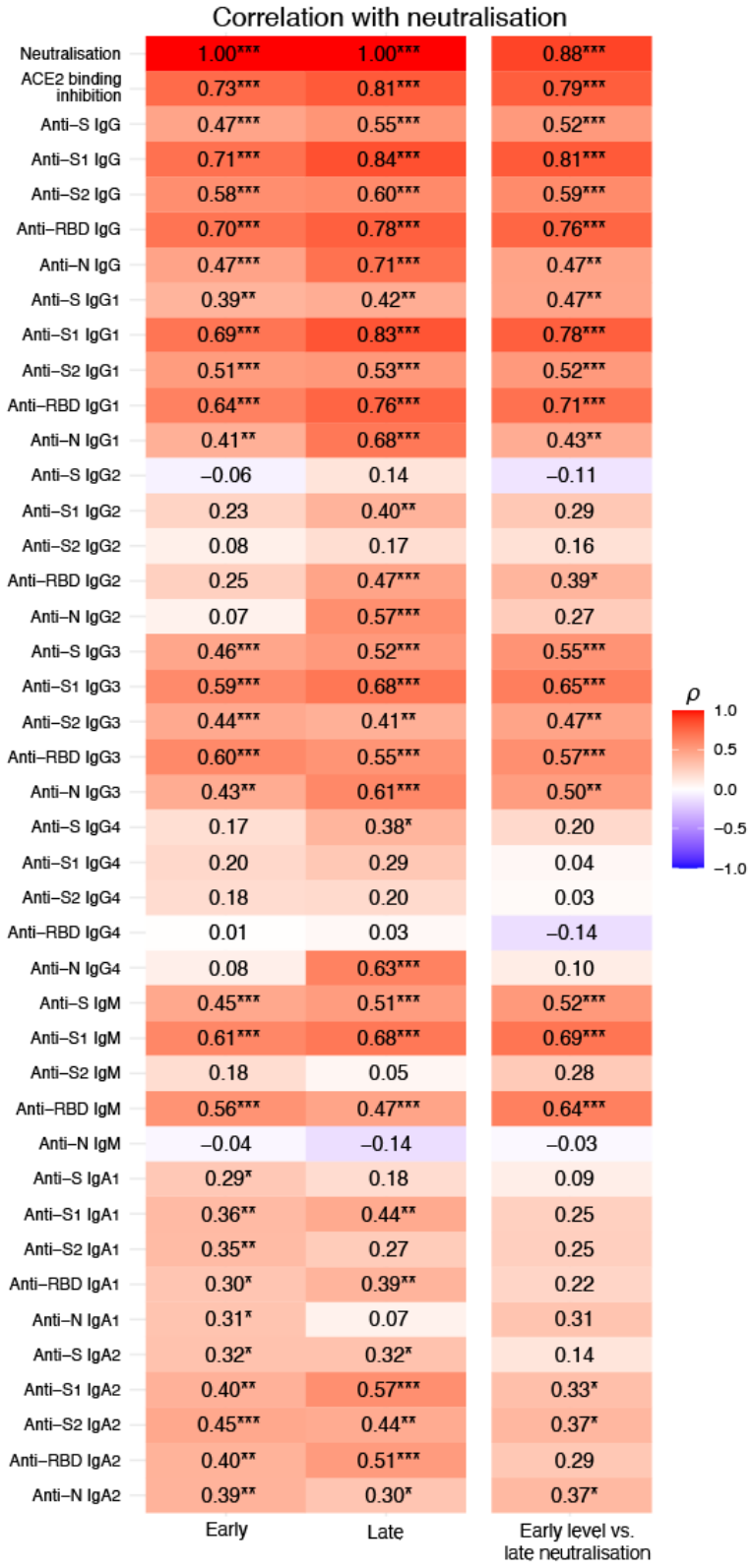

Extended Data Figure 3: Correlation of antibody binding and ACE2 inhibition with neutralisation.

A heat-map of Spearman correlations between neutralisation titre and the serological measurements of antibody binding (by isotype and antigen). Correlations were assessed in early (≤50 days, left column n=54 subjects) and late (≥100 days, right middle column, n=47 subjects) convalescence in all subjects were data was available. The association between early antibody binding and late neutralisation is also shown (right column, n=47 subjects). All correlations are Spearman correlations. *P≤0.05, **P≤0.01, ***P≤0.001.

A

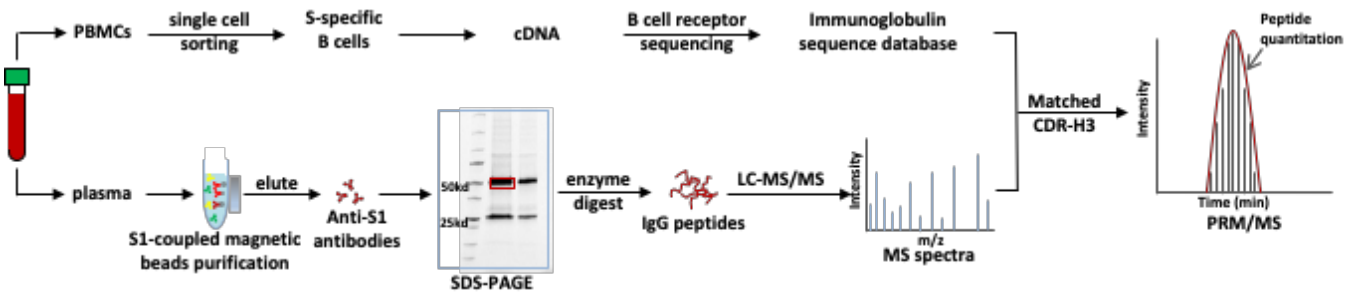

B

Subject	IGHV	IGHD	IGHJ	Translated CDR-H3 sequences	Matched CDR-H3 peptide sequences
CP04	1-3	3-10	6	ARILGTTRKYFDDSERDGMDVW	KYFDDSERDGMDVWGQGTTVTVSSASTK (pep1) KYFDDSER (pep2)
	4-34	3-22	4	ARDRYHYYDSSGYSKNYRHFDYW	DRYHYYDSSGYSK (pep3)
CP08	1-69	3-10	6	VRGMYASGNYRGSDFFYGMDVW	GMYASGNYR (pep4)
				VRGLYASGNFRGSDFFYGMDVW	GLYASGNFR (pep5)
				VRGLYASGSYRGSDFFYGMDVW	GLYASGSYR (pep6)
	1-69	6-13	6	ARVGAPIERTSSSWHYYYYGMDVW	VGAPIER (pep7)
	4-31	6-6	4	ARGFYEVYSSPTIKEYYFDYW	GFYEVYSSPTIK (pep8)
	3-7	3-16	4	ARVKINPYYDYVWGSYRYSRILDYW	YDYVWGSYR (pep9)
CP63	1-69	3-22	4	ARLGRGDYDSSGYYKVYFDYW	GDYDSSGYYK (pep10)
FCP01	1-46	3-10	6	SRGITLVQGVVRALRPGSKEYYYYGLDVW	YCSRGITL (pep11) GITLVQGVVR (pep12) GFTLVQGVVR (pep13) VQGVVRAL (pep14) ALRPGSKEYY (pep15) TLVQGVVR (pep16)

C

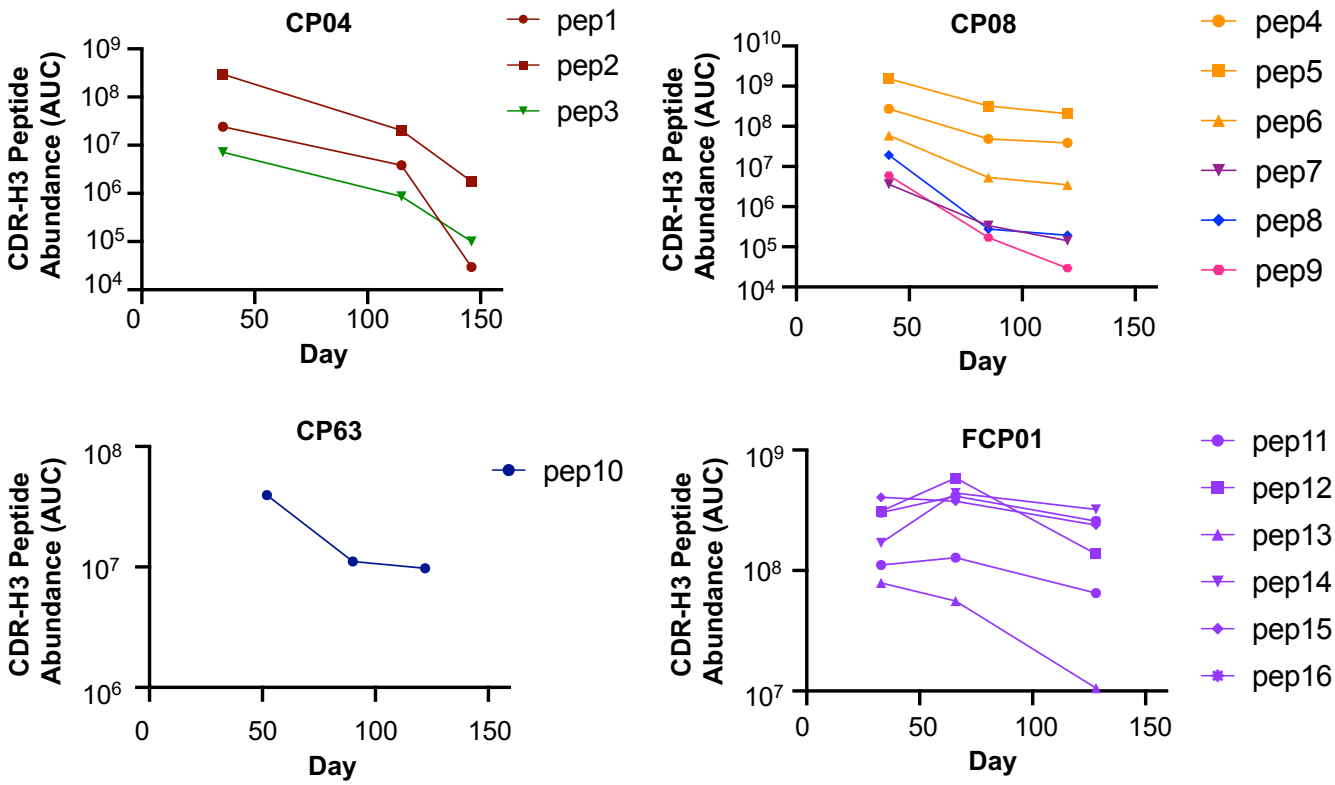

Extended Data Figure 4: MS-based quantification of immunoprecipitated S1-specific clonotypic antibodies.

(**A**) Combined B cell receptor sequencing and proteomics platform enables identification and quantification of circulating anti-S1 antibodies. S1-specific IgG was purified from plasma of SARS-CoV-2 convalescent subjects using antigen-coupled magnetic beads and heavy chains subject to LC-MC/MS. Peptide spectra are searched against B-cell receptor sequencers recovered from single sorted S-specific memory B cells from matched individuals to identify clonotypes based upon CDR-H3 amino acid sequence. Clonotype specific peptides are then used as barcodes for relative quantitative parallel reaction monitoring (PRM) for tracking in longitudinal plasma samples. Targeted peptides are monitored during elution from HPLC and individual peptides quantified based on abundance chromatography curves. (**B**) Clonotypes identified based on matched CDR-H3 sequences from S1-specific plasma IgG and B cell receptor sequences from SARS-CoV-2 convalescent subjects (n=4). (**C**) Longitudinal changes in the relative plasma abundance of anti-S1 clonotypes within four convalescent subjects over time. The quantity of each reference peptide is expressed as area under the curve (AUC) derived from extracted ion chromatography.

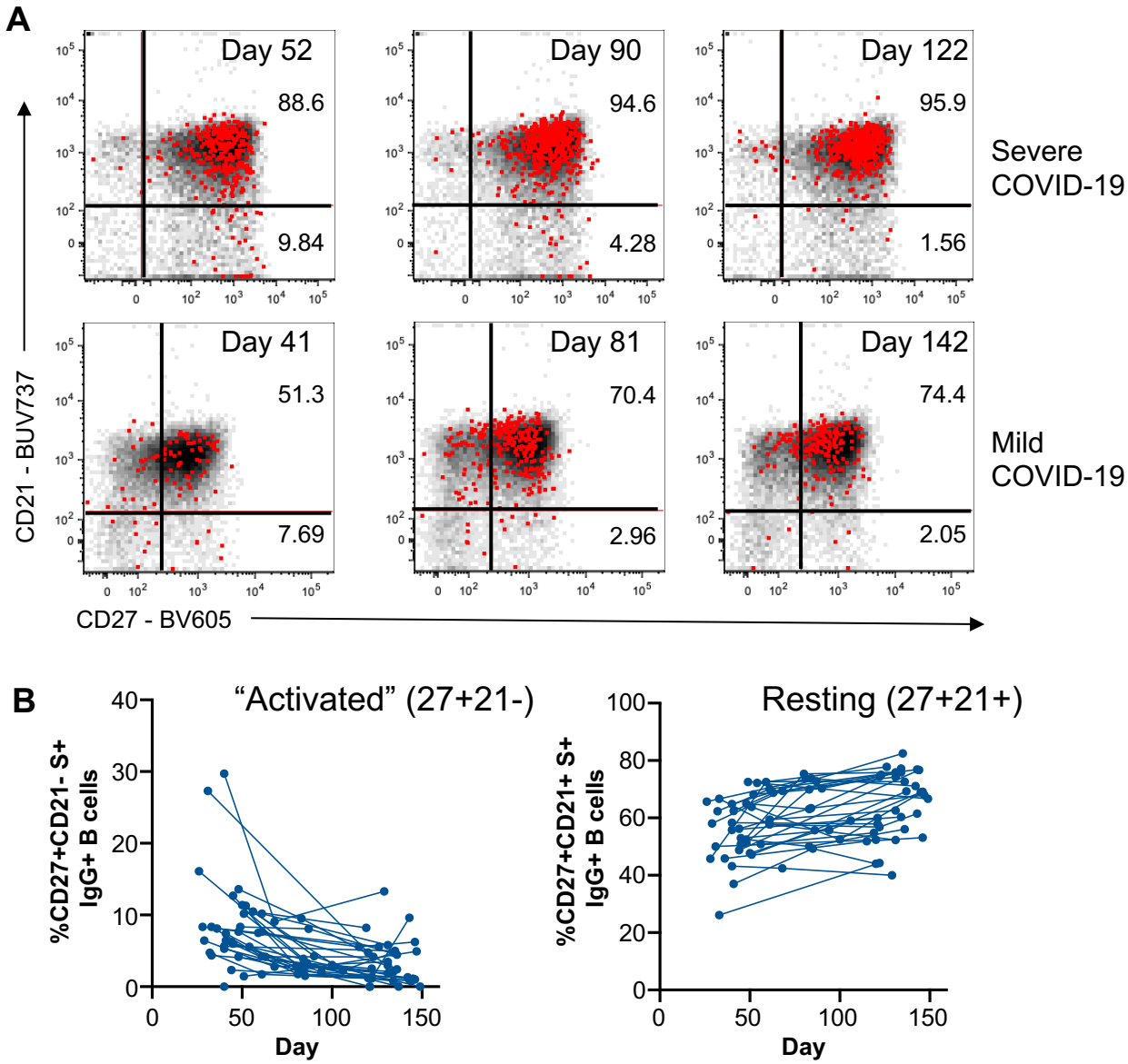

Extended Data Figure 5: Activation status of S-specific IgG+ memory B cells.

(**A**) Memory B cell phenotypes identified by CD21 and CD27 co-staining of S+CD19+CD20+IgD-IgG+ B cells (red) overlaid onto parental CD19+CD20+IgD-IgG+ B cells (black) and (**B**) the corresponding frequencies of "activated" (CD27+CD21-) or resting (CD27+CD21+) in in PBMC samples were assessed longitudinally (n=31 subjects).

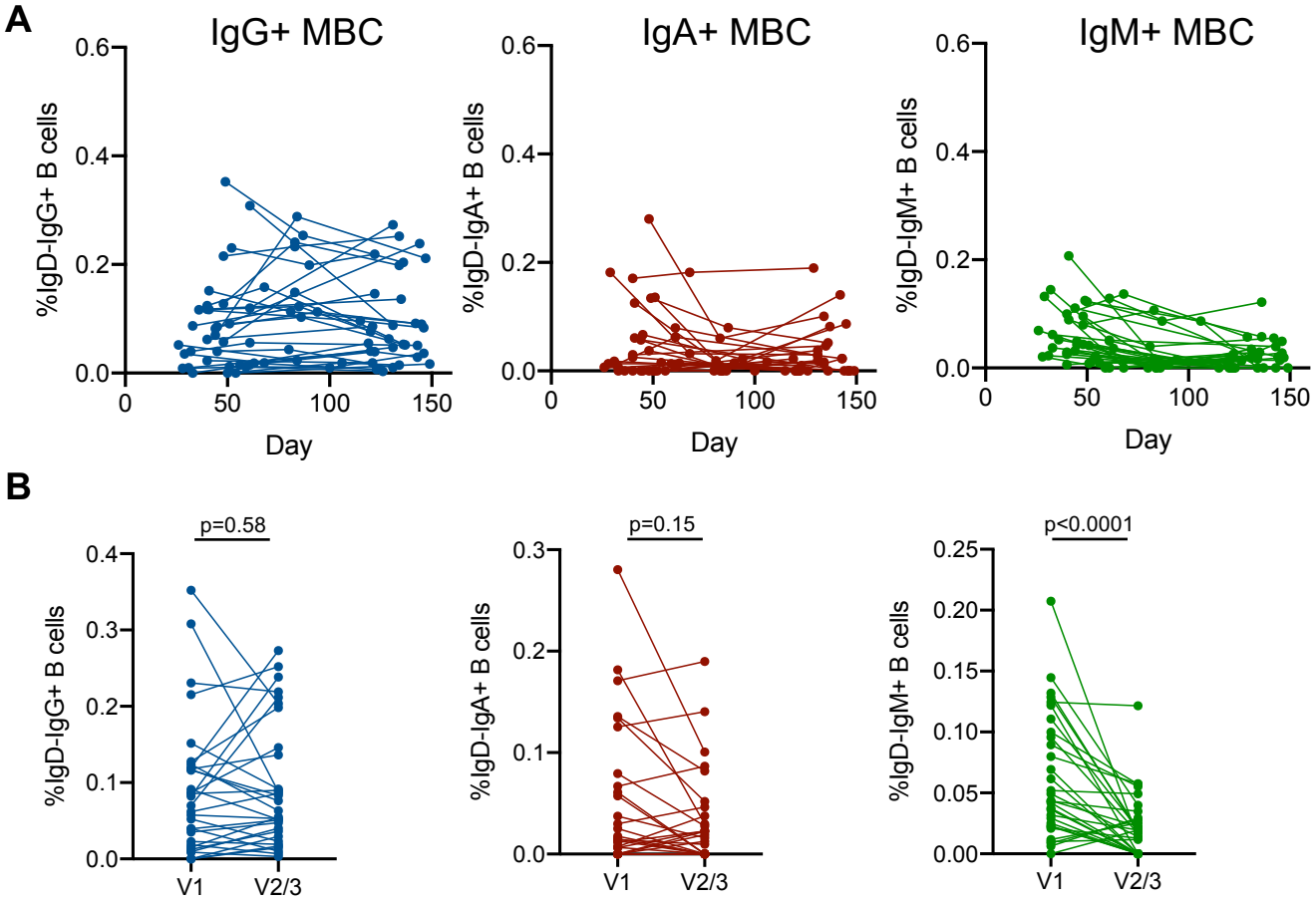

Extended Data Figure 6: RBD-specific memory B cell dynamics.

(**A**) Frequencies of RBD-specific IgG+, IgA+ or IgM+ memory B cells as a proportion of CD19+CD20+IgD- B cells in PBMC samples were assessed longitudinally. (**B**) Comparison of RBD-specific IgG+, IgA+ or IgM+ memory B cell frequencies at the earliest and latest timepoint available for each individual (n=31). Statistics assessed by two-tailed Wilcoxon test.

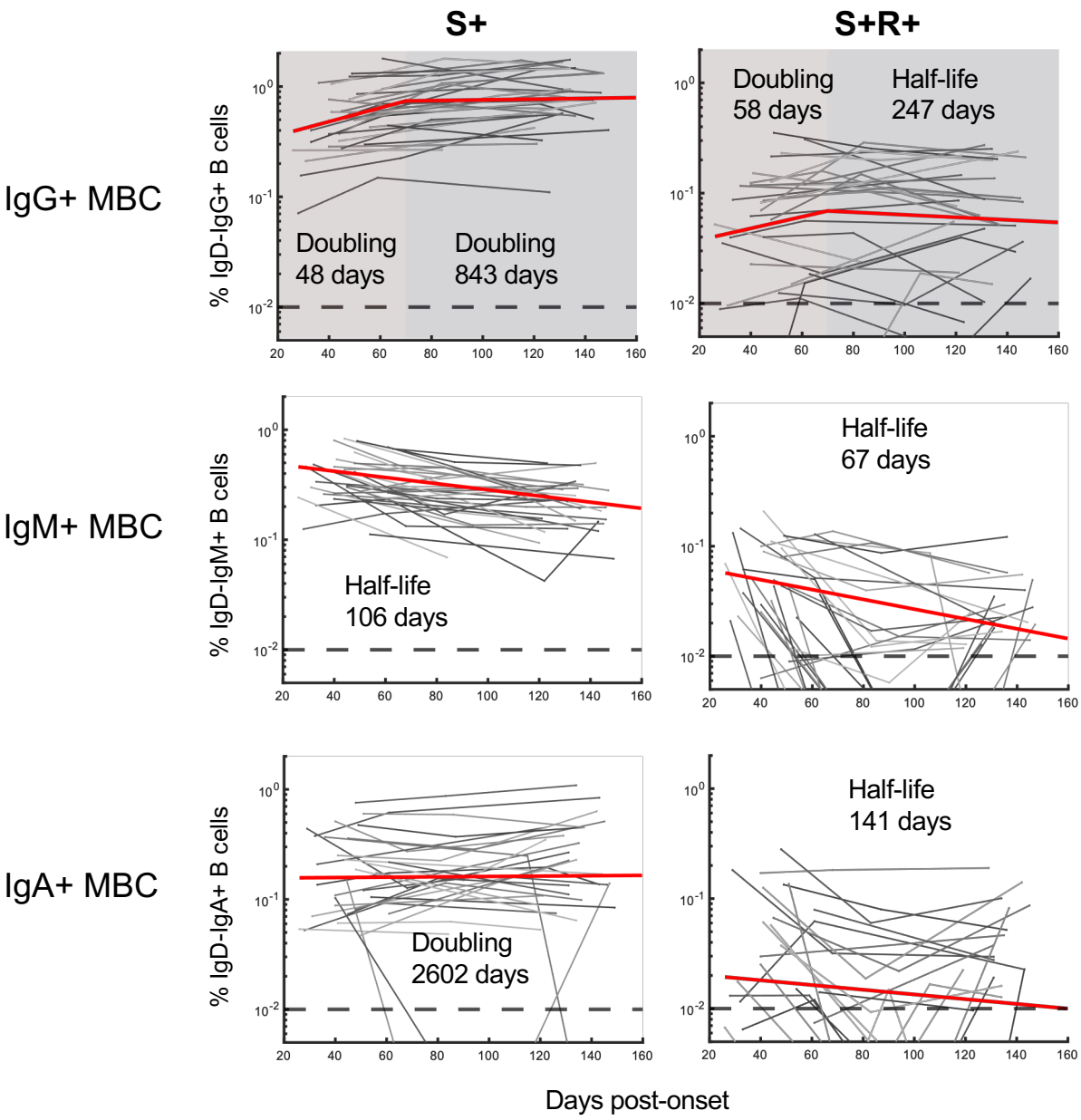

Extended Data Figure 7: Fitting of the kinetics of S- and RBD-specific memory B cell responses over time.

The best-fit half-lives are shown for the fitting of the growth and/or decay of S- or RBD-specific memory B cells (n=31 subjects). Two-phase decay is indicated by red (before day 70) and blue (after day 70) shaded areas. No shading indicates where a single-phase decay model was used to fit the data.

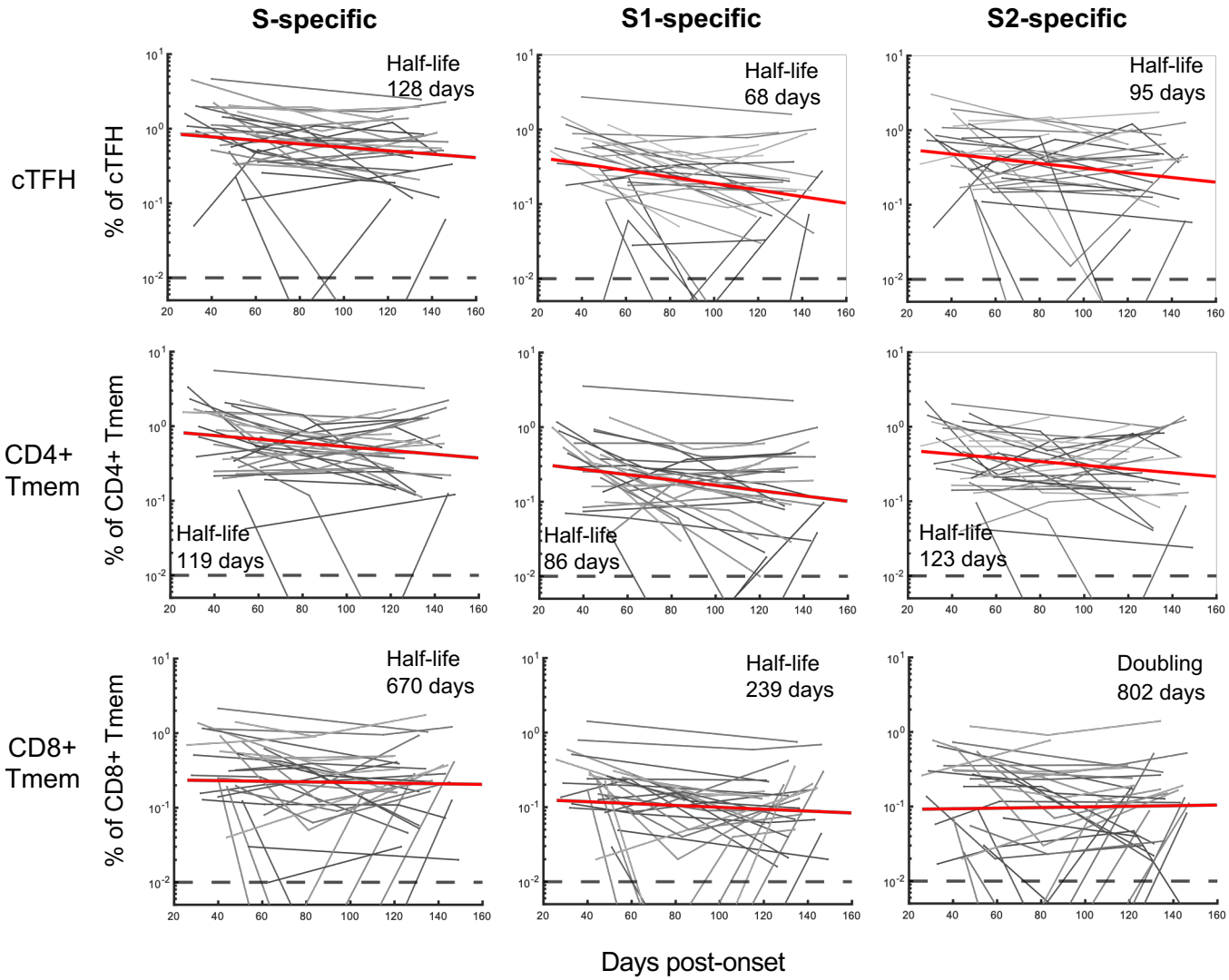

Extended Data Figure 8: Fitting of the decline in SARS-CoV-2-specific T cells over time.

The best-fit half-lives are shown for the fitting of the decay of cTFH, CD4+ Tmem and CD8+ Tmem specific to total S (S1+S2 responses combined), S1 or S2 peptide pools (n=31 subjects). In all cases decay was fit with a single-phase decay model with the half-lives shown.

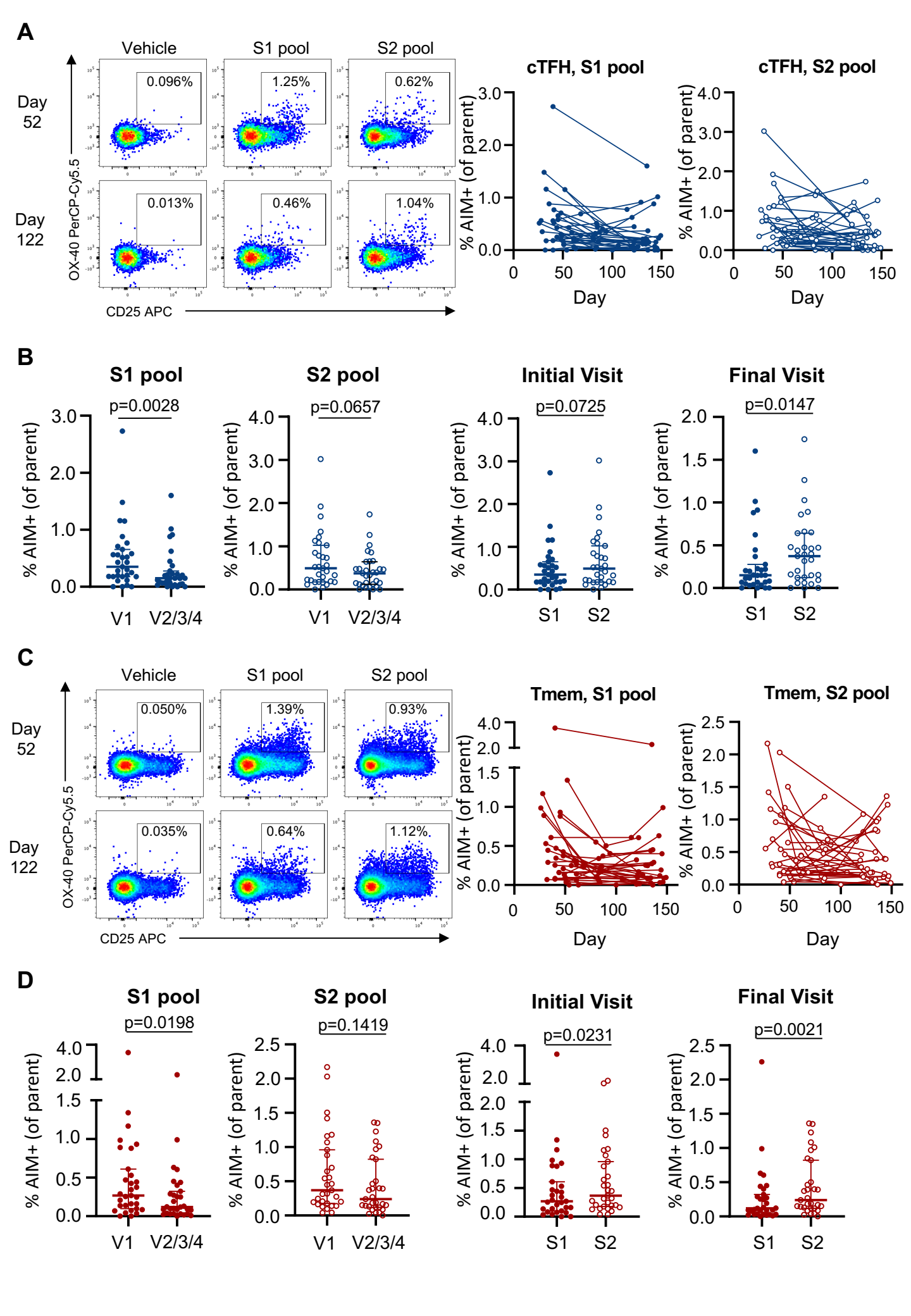
A
Vehicle
S1 pool
S2 pool
Day 52
Day 122
0.096%
1.25%
0.62%
0.013%
0.46%
1.04%
OX-40 PerCP-Cy5.5
CD25 APC
cTFH, S1 pool
cTFH, S2 pool
% AIM+ (of parent)
Day
B
S1 pool
S2 pool
Initial Visit
Final Visit
p=0.0028
p=0.0657
p=0.0725
p=0.0147
V1
V2/3/4
S1
S2
C
0.050%
1.39%
0.93%
0.035%
0.64%
1.12%
Tmem, S1 pool
Tmem, S2 pool
D
p=0.0198
p=0.1419
p=0.0231
p=0.0021

Extended Data Figure 9: S1 and S2-specific CD4+ T cell responses.

(**A, C**) Representative staining of AIM markers following S1 and S2 peptide pool stimulation among (**A**) cTFH (CD3+CD4+CD8-CD45RA-CXCR5+) or (**C**) CD4+ Tmem cells and longitudinal cohort analysis (n=31). (**B, D**) Comparison of S1 or S2-specific (**B**) cTFH or (**D**) CD4+ Tmem responses at the earliest and latest visit for each participant, as well as paired frequency of S1 versus S2 responses at the initial or final visit (n=31). Statistics assessed by two-tailed Wilcoxon test.

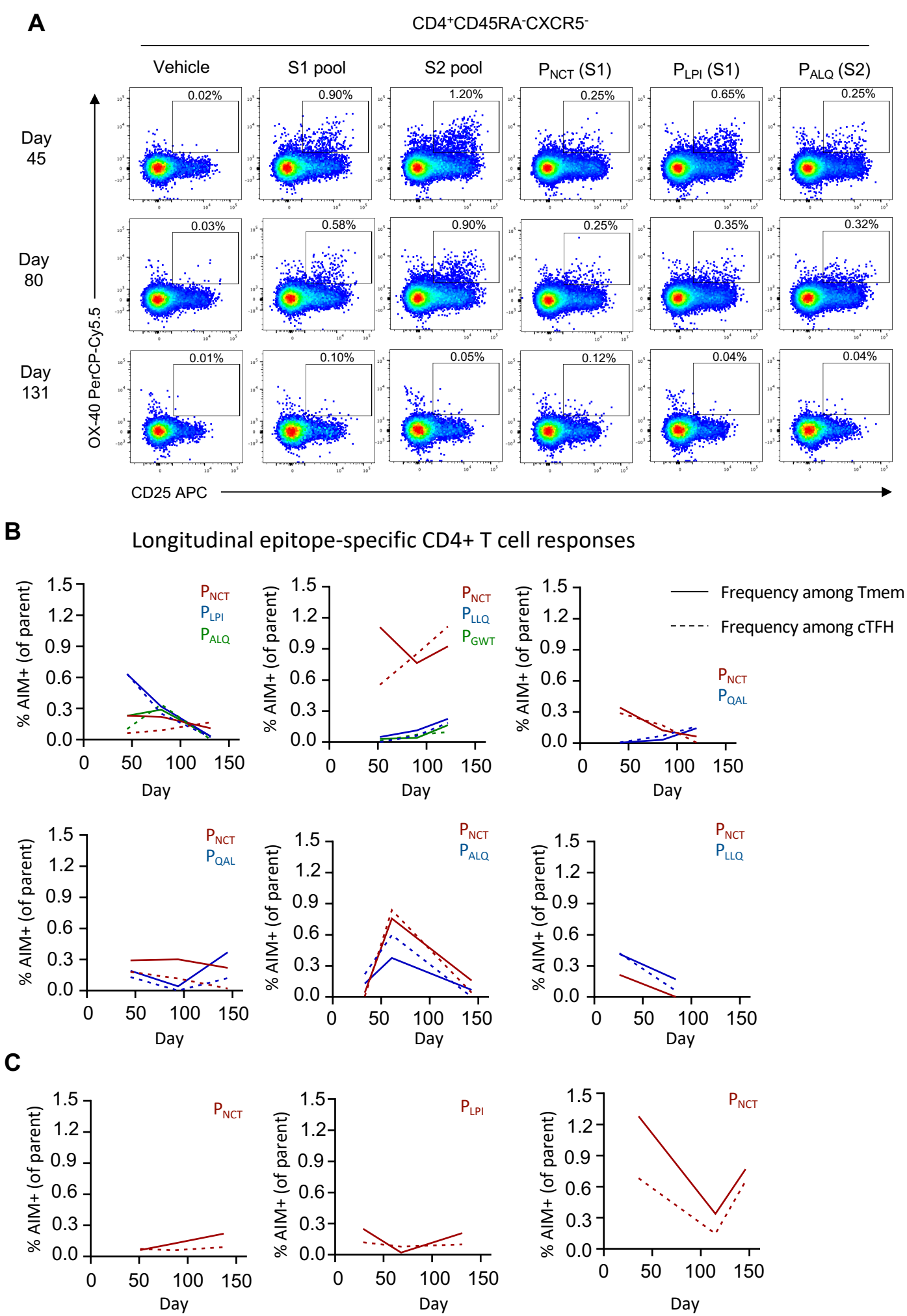
A
CD4+CD45RA-CXCR5-
Vehicle
S1 pool
S2 pool
PNCT (S1)
PLPI (S1)
PALQ (S2)
Day 45
Day 80
Day 131
0.02%
0.90%
1.20%
0.25%
0.65%
0.25%
0.03%
0.58%
0.90%
0.25%
0.35%
0.32%
0.01%
0.10%
0.05%
0.12%
0.04%
0.04%
OX-40 PerCP-Cy5.5
CD25 APC
B
Longitudinal epitope-specific CD4+ T cell responses
% AIM+ (of parent)
Day
PNCT
PLPI
PALQ
PLLQ
PGWT
PQAL
Frequency among Tmem
Frequency among cTFH
C

Extended Data Figure 10: Epitope-specific CD4+ T cell responses.

(**A**) Representative staining of AIM markers following S1 or S2 peptide pool or individual peptide stimulation among the CD4+ Tmem population. (**B,C**) Longitudinal peptide-specific frequencies in individual subjects (n=9; solid line, CD4+ Tmem; dashed line, cTFH) for whom (**B**) multiple or (**C**) single epitopes were identified.

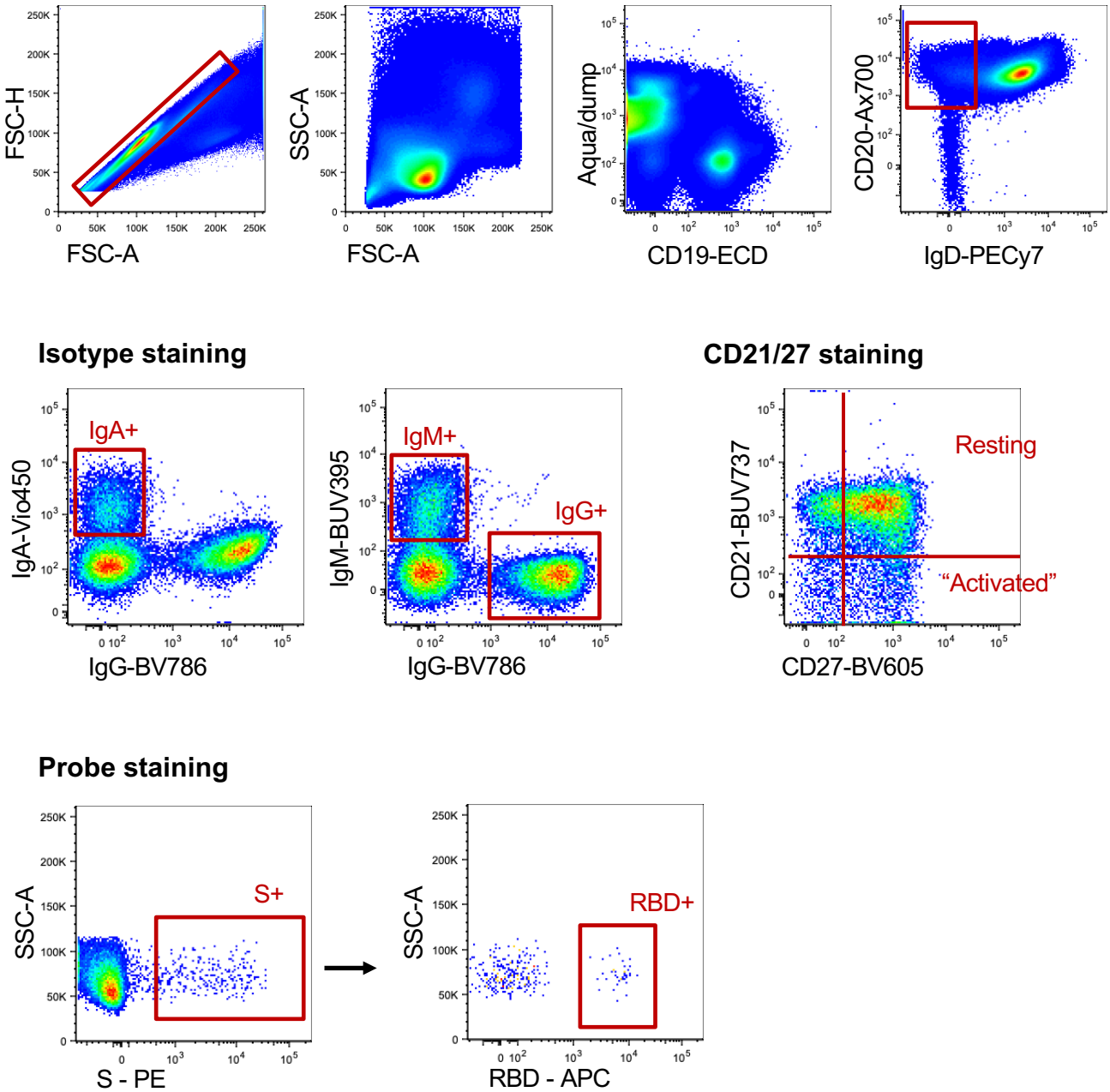

Supplementary Fig. S1: Gating strategy for resolving antigen-specific B cells and surface isotypes.

After doublet exclusion (FSC-A vs FSC-H) and lymphocyte gating (FSC-A vs SSC-A), live CD19+IgD-CD20+ B cells were gated based on surface immunoglobulin expression (IgM, IgG, IgA). Binding to SARS-CoV-2 spike (S) and/or SARS-CoV-2 RBD probes was assessed for each population. Memory B cell phenotypes were identified by CD21 and CD27 co-staining.

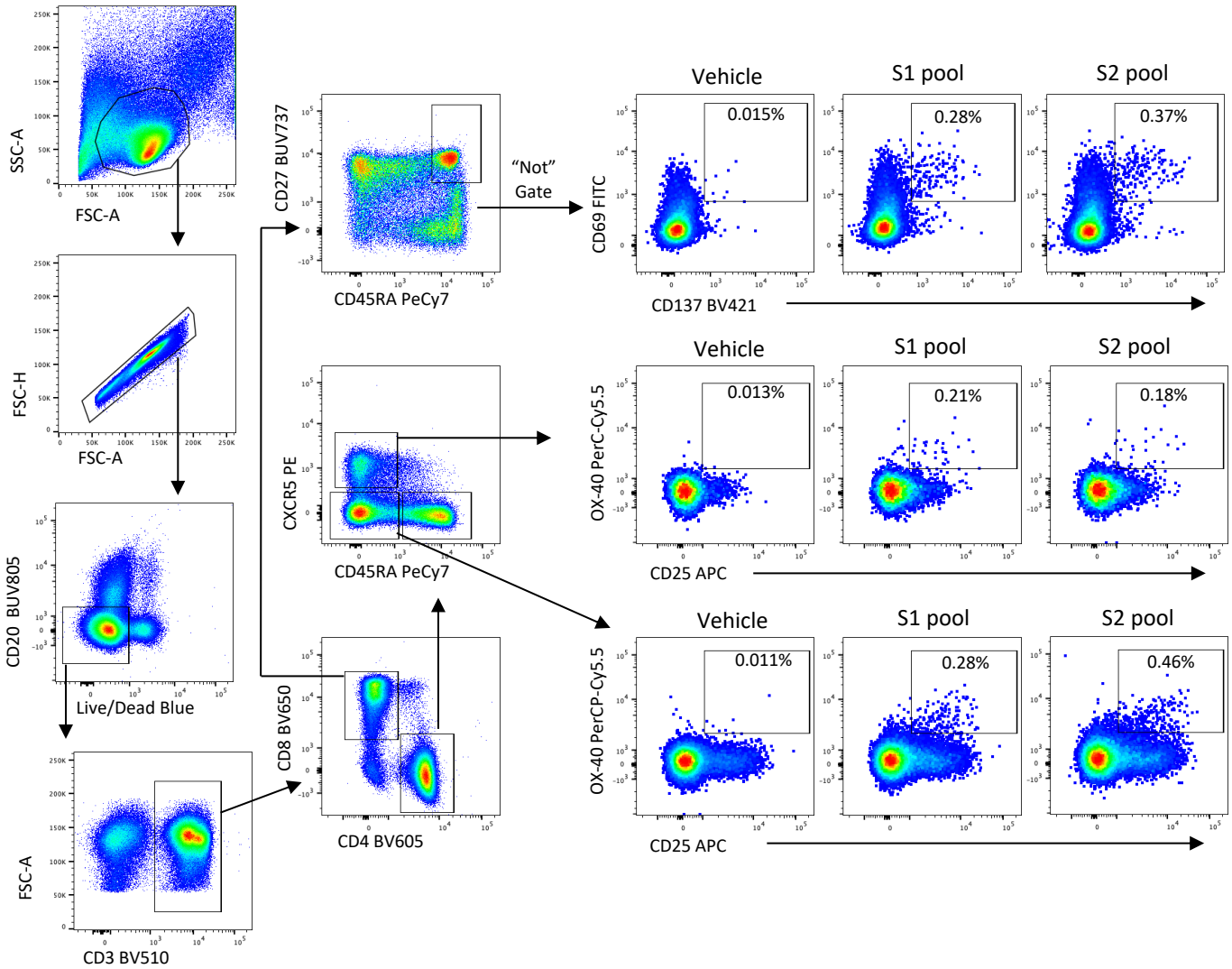

Supplementary Fig. S2: Gating strategy for quantifying antigen-specific T cells. Lymphocytes were identified by FSC/SSC, followed by doublet exclusion (FSC-A vs FSC-H), and exclusion of dead or CD20+ cells. After gating on CD3, single positive CD4 or CD8 T cell subsets were identified. CD8 Tmem were gated as non-naïve (CD27+CD45RA+) cells, and assessed for co-expression of CD69 and CD137 following stimulation. CD4 T cells were gated as cTFH (CXCR5+CD45RA-) or Tmem (CXCR5-CD45RA-), and assessed for co-expression of OX-40 and CD25 following stimulation.

Pep1 Intensity **KYFDDSERDGMDVWGQGTTVTVSSASTK** m/z = 1033.7998 (z = 3)

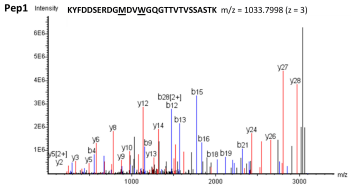

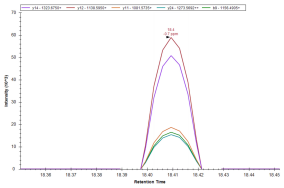

Pep2 Intensity **KYFDDSER** m/z = 558.7517 (z=2)

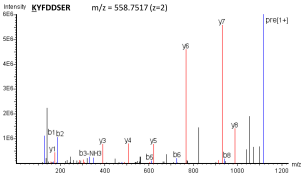

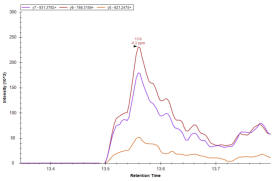

Pep3 Intensity **DRYHYYDSSGYSK** m/z = 547.5707 (z = 3)

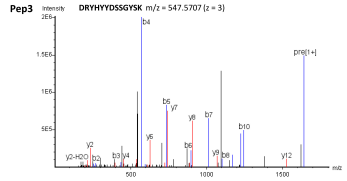

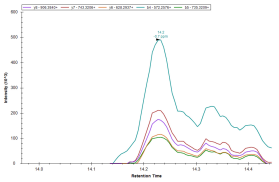

Pep4 Intensity **GMYASGNYR m/z = 517.72 (z = 2)**

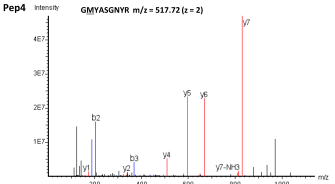

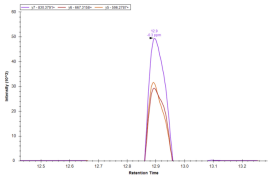

Pep5 Intensity **GLYASGNFR m/z = 492.7485 (z = 2)**

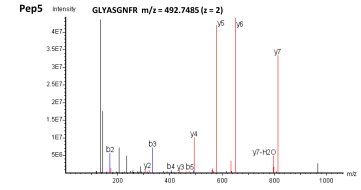

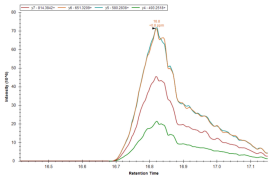

Pep6 Intensity **GLYASGSYR** m/z = 487.2405 (z = 2)

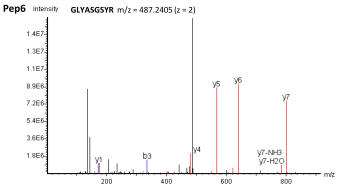

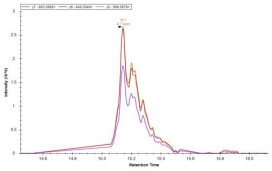

Pep7 Intensity **VGAPIER** m/z = 371.2163 (z = 2)

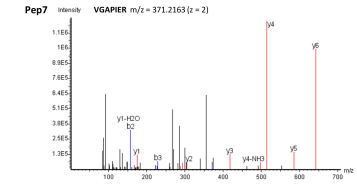

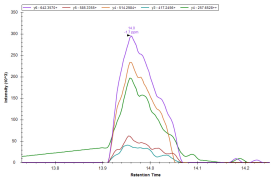

Pep8 Intensity **GFYEVYSSPTIK** m/z = 695.8481 (z = 2)

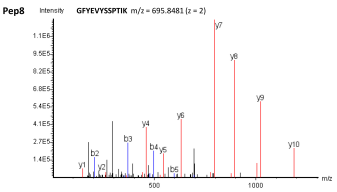

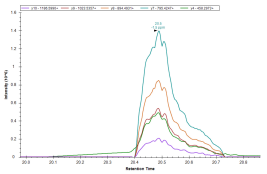

Pep9 Intensity **YDYVWGSYR** m/z = 654.2882 (z = 2)

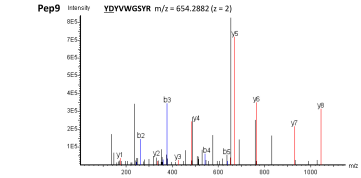

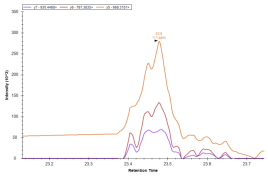

Pep10 Intensity **GDYDSSGYYK** m/z = 577.7355 (z = 2)

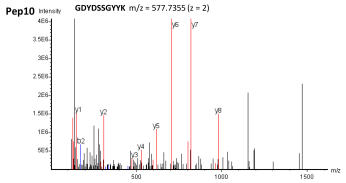

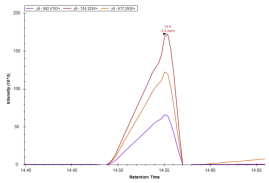

Pep11 Intensity **YCSRGITL** m/z = 485.2448 (z = 2)

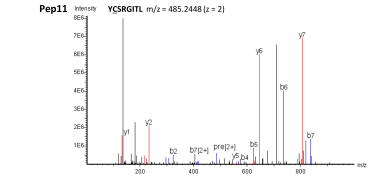

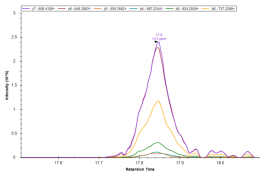

Pep12 Intensity **GITLVQGVVR** m/z = 521.3244 (z = 2)

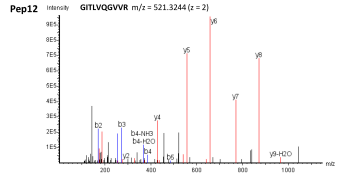

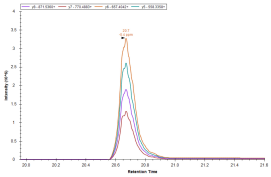

Pep13 Intensity **GFTLVQGVVR** m/z = 538.3166 (z = 2)

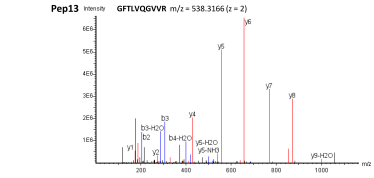

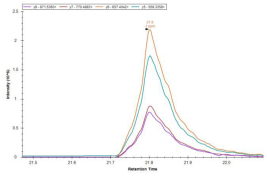

Pep14 Intensity **VQGVVRAL** m/z = 421.2663 (z = 2)

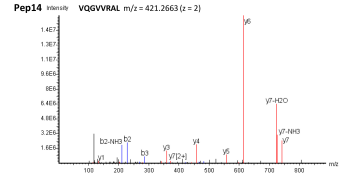

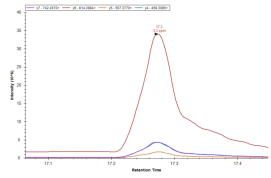

Pep15 Intensity **ALRPGSKEYY** m/z = 395.2084 (z = 3)

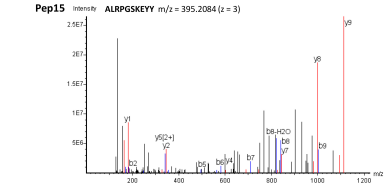

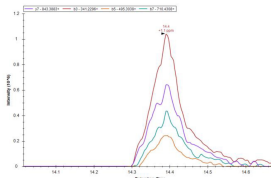

Pep16 Intensity **TLVQGVVR** m/z = 436.2716 (z = 2)

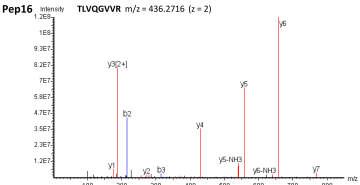

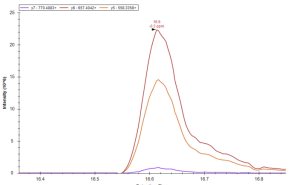

Supplementary Fig. S3: Representative annotated MS/MS spectra (left panel) and their corresponding extracted ion chromatograms (XICs; right panel). The peptides used in PRM analyses are the matched clonotypic CDR-H3 peptides (pep1-16). Underlined amino acid indicates a post translational modification: M (oxidised methionine), W (oxidised tryptophan), K (carbamidomethylated lysine), D (carbamidomethylated aspartate), C (carbamidomethylated cysteine), and Y (acetylated tyrosine). The sequences, m/z and z of each individual peptides are shown on the top of their annotated MS/MS spectra. Matched b ions are indicated in blue and y ions are in red. m=mass, z=charge.